2012

Effects of Ring Exchange Interaction on the Néel Phase of Two-dimensional, Spatially Anisotropic, Frustrated Heisenberg Quantum Antiferromagnet

Kingshuk Majumdar
Grand Valley State University, majumdak@gmail.com

Douglas Furton
Grand Valley State University, furtond@gvsu.edu

Götz S. Uhrig
Technische Universität Dortmund

Effects of ring exchange interaction on the Néel phase of two-dimensional, spatially anisotropic, frustrated Heisenberg quantum antiferromagnet

Kingshuk Majumdar* and Douglas Furton†

Department of Physics, Grand Valley State University, Allendale, Michigan 49401, USA

Götz S. Uhrig

Lehrstuhl für Theoretische Physik I, Technische Universität Dortmund,

Otto-Hahn Straße 4, 44221 Dortmund, Germany‡

(Dated: April 25, 2012)

Abstract

Higher order quantum effects on the magnetic phase diagram induced by four-spin ring exchange on plaquettes are investigated for a two-dimensional quantum antiferromagnet with $S = 1/2$. Spatial anisotropy and frustration are allowed for. Using a perturbative spin-wave expansion up to second order in $1/S$ we obtain the spin-wave energy dispersion, sublattice magnetization, and the magnetic phase diagram. We find that for substantial four-spin ring exchange the quantum fluctuations are stronger than in the standard Heisenberg model. A moderate amount of four-spin ring exchange couplings stabilizes the ordered antiferromagnetic Néel state while a large amount renders it unstable. Comparison with inelastic neutron scattering data points toward a moderate ring exchange coupling of 27% to 29% of the nearest-neighbor exchange coupling.

PACS numbers: 75.10.Jm, 75.40.Mg, 75.50.Ee, 73.43.Nq

I. INTRODUCTION

Despite the intense experimental and theoretical activities to understand the origin of high temperature superconductivity in layered oxide high-temperature superconductors, the underlying microscopic mechanism is still incomplete.[1–9] Very recently the crucial role of magnetic excitations in these compounds has been supported by their observation in the whole Brillouin zone up to high energies and high levels of doping.[10]

The conventional route to theoretically investigate the magnetic properties of these undoped compounds is the two-dimensional (2D) antiferromagnetic (AF) spin-1/2 Heisenberg model with nearest neighbor (NN) AF coupling J_1 and next-nearest neighbor (NNN) antiferromagnetic coupling J_2.[11] For concreteness, we give the studied Heisenberg Hamiltonian for a $S = 1/2$ antiferromagnet on a square lattice

$$\begin{aligned} H &= \frac{1}{2}J_1 \sum_i \mathbf{S}_i \cdot \mathbf{S}_{i+\delta_x} + \frac{1}{2}J_1' \sum_i \mathbf{S}_i \cdot \mathbf{S}_{i+\delta_y} + \frac{1}{2}J_2 \sum_i \mathbf{S}_i \cdot \mathbf{S}_{i+\delta_x+\delta_y} \\ &+ 2K \sum_i \Big[(\mathbf{S}_i \cdot \mathbf{S}_{i+\delta_x})(\mathbf{S}_{i+\delta_y} \cdot \mathbf{S}_{i+\delta_x+\delta_y}) + (\mathbf{S}_i \cdot \mathbf{S}_{i+\delta_y})(\mathbf{S}_{i+\delta_x} \cdot \mathbf{S}_{i+\delta_x+\delta_y}) \\ &- (\mathbf{S}_i \cdot \mathbf{S}_{i+\delta_x+\delta_y})(\mathbf{S}_{i+\delta_y} \cdot \mathbf{S}_{i+\delta_x}) \Big]. \end{aligned} \tag{1}$$

We consider four different exchange couplings: J_1 for nearest neighbors (NN) along the rows, J_1' for NN along the columns, J_2 for the next nearest neighbors (NNN) along the diagonals, and finally the four-spin ring exchange interaction K. All interactions are assumed to be antiferromagnetic, i.e., $J_1, J_1', J_2, K > 0$. Here i runs over N lattice sites and δ_x, δ_y are unit vectors in both directions. In the present work, we study the parameter region where the ground state is of Neél type as shown in Fig. 1. We take J_1 as the fundamental energy scale so that the ground state and its properties depend on the dimensionless ratio $\eta := J_2/J_1$ parametrizing the degree of frustration, the ratio $\zeta := J_1'/J_1$ parametrizing the degree of spatial anisotropy, and the ratio $\mu = KS^2/J_1$ parametrizing the relative strength of the four-spin ring exchange. Note that the full cyclic permutation around a plaquette comprises also two-point couplings along the plaquette edges and along the diagonals.[12] But they do not need to be considered separately because they are incorporated in J_1, J_1', and J_2.

Experimentally the ground state phase diagram of these frustrated spin systems can be explored from high values to low values of η by applying high pressures. For example, X-ray diffraction measurements on Li_2VOSiO_4 show that the value of η decreases by about 40%

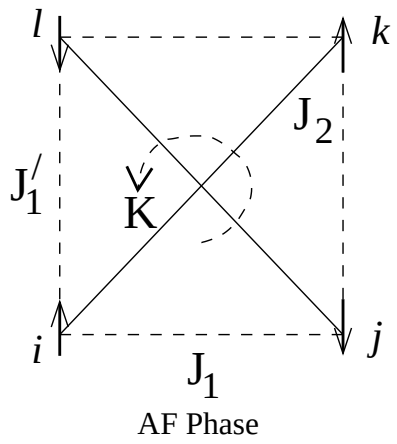

FIG. 1: Classical antiferromagnetic ground state (Néel state) and the various couplings: J_1, J_1' are nearest neighbor interactions along the row and column directions respectively, J_2 is the next-nearest neighbor interaction along the diagonals, and K is the cyclic four-spin ring exchange. All couplings are assumed to be antiferromagnetic, i.e., $J_1, J_1', J_2, K > 0$.

with increase in pressure from zero to 7.6 GPa.[13]

Theoretically, evidence for sizable four-spin ring exchange K in high-temperature superconductors[14–16] was found soon after the discovery of high-temperature superconductivity.[17] Such exchange processes turned out to be the dominant subleading correction to the NN Heisenberg Hamiltonian if it is derived from a three-band Hubbard model[18–20] or from a single-band Hubbard model[21–24]. Experimental evidence for ring exchange stems from the analysis of infrared absorption[25], of Raman response[26,27], and of inelastic neutron scattering[1,2,28,29]. The results indicate that the ring exchange coupling reaches between $x_{\rm ring} = 2K/J_1 = 0.2$ and 0.25 relative to the NN coupling. Note that for $S = 1/2$ one has $x_{\rm ring} = 8\mu$. These findings and the quantitative estimates are strongly supported by the analysis of two-leg spin ladder systems such as $Sr_{14}Cu_{24}O_{41}$, $Ca_8La_6Cu_{24}O_{41}$, and $(Ca, La)_{14}Cu_{24}O_{41}$.[12,27,30–33]

The recent discovery of superconductivity in the class of iron pnictide has ushered a renewed interest in this exciting field.[34] The parent phases of these materials have been found to be metallic, but with columnar AF order.[35–37]. Since the superconductivity appears in immediate proximity of the magnetically ordered phase, it is evident that the magnetic excitations play an important role.[38–40] Neglecting the metallicity of the parent phases the magnetic excitations can be described by frustrated two-dimensional Heisenberg Hamiltoni-

ans with $S > 1/2$[41–44] although the three-dimensionality cannot be neglected[45–48]. Ab initio calculations seem to indicate a strong spatial anisotropy $\zeta \approx 0$ of the NN couplings[49] fitting to the experimental findings.[38–40] But the weak structural distortion does not explain this strong anisotropy. So either orbital order[50,51] or higher order magnetic exchange such as NN biquadratic coupling[52–55] may effectively explain the anisotropy.

Another class of magnetic materials described by the Hamiltonian in Eq. (1) are vanadium phosphates. Extensive band structure calculations[56] yielded four different exchange couplings: J_1 and J_1' between the NN and J_2 and J_2' between NNN in the compounds $Pb_2VO(PO_4)_2$, $SrZnVO(PO_4)_2$, $BaZnVO(PO_4)_2$, and $BaCdVO(PO_4)_2$. For example $\zeta \approx 0.7$ and $J_2'/J_2 \approx 0.4$ were obtained for $SrZnVO(PO_4)_2$. Also the compound $(NO)Cu(NO_3)_3$ possibly realizes the J_1-J_1'-J_2 model.[57]

The above examples corroborate the relevance of the model (1).

It is now well known that at low temperatures the spin-1/2 antiferromagnetic J_1-J_2 model on a square lattice exhibits new types of magnetic order and novel quantum phases.[11] For $J_2 = 0$ and $K = 0$ the ground state is Néel ordered at zero temperature. Addition of next-nearest neighbor (NNN) interactions induces a strong frustration and breaks the Néel order at a quantum critical point $J_2/J_1 \approx 0.4$ as found by $1/S$ expansions[58–60], series expansion about the Ising limit[61], and the coupled-cluster approach[62]. We stress that the precise nature of the phase beyond the Néel phase is still intensely debated[63–65].

A generalization of the frustrated J_1-J_2 model is the J_1-J_1'-J_2 model where $\zeta = J_1'/J_1$ is the directional anisotropy parameter.[59,60,66] Recently, the role of directional anisotropy on the magnetic phase diagram has been investigated in detail using a spin-wave expansion.[60]

The next generalization consists in the inclusion of the four-spin ring exchange interaction K which is the next important coupling after the NN exchange coupling. Using linear spin-wave theory its effects on the magnetic properties of the J_1-J_2-K model were studied in Ref. 16 where a quasiclassical phase diagram in $\mathcal{O}((1/S)^0)$ was obtained. In Ref. 28 corrections to the spin-wave spectrum to first order in $1/S$ were studied for finite K using self-consistent spin-wave theory. The self-consistent spin-wave theory is a mean-field approach which captures only a part of the second-order effects $\mathcal{O}((1/S)^2)$ in the phase diagram. In particular, it does not take virtual excitations of two and four magnons into account. To consider them a perturbative spin-wave expansion up to $1/S^2$ is needed. That is the goal of the present work.

In the present paper we investigate the higher-order quantum corrections due to the presence of plaquette four-spin ring interactions on the antiferromagnetic phase diagram of the J_1-J_1'-J_2-K Heisenberg model on a square lattice, cf. Eq. (1). Our calculations use the Dyson-Maleev spin representation which facilitates the calculation significantly compared to the Holstein-Primakov representation. The concomitant formalism is presented in the next section. Results for the spin-wave energies and the magnetizations of the system are presented and discussed in Section III. A quantitative comparison with experimental data is also included. Section IV contains a brief summary of our results.

II. FORMALISM

Quantum fluctuations play a significant role in the magnetic phase diagram of the system at zero temperature. We will investigate the role of quantum fluctuations on the stability of the Néel phase. We first express the fluctuations around the classical antiferromagnetic ground state in terms of the boson operators using the Dyson-Maleev representation. The quadratic term in boson operators corresponds to the linear spin-wave theory, whereas the higher-order terms represent spin-wave interactions and virtual processes. We keep terms up to second order in $1/S$. In the next step we calculate the renormalized magnon Green's functions and self-energies. Finally, we calculate the magnon energy dispersion and the sublattice magnetization up to and including terms of order $1/S^2$.

For the Néel ordered phase NN couplings interact between the A and B sublattices while NNN couplings link A and A sites or B and B sites, respectively. The Hamiltonian in Eq. (1) takes the form

$$\begin{aligned} H \;=\; & J_1 \sum_i \mathbf{S}_i^{\mathrm{A}} \cdot \mathbf{S}_j^{\mathrm{B}} + J_1' \sum_i \mathbf{S}_i^{\mathrm{A}} \cdot \mathbf{S}_\ell^{\mathrm{B}} + \frac{1}{2} J_2 \sum_i \Big[\mathbf{S}_i^{\mathrm{A}} \cdot \mathbf{S}_k^{\mathrm{A}} + \mathbf{S}_j^{\mathrm{B}} \cdot \mathbf{S}_\ell^{\mathrm{B}} \Big] \\ & + \; 2K \sum_i \Big[(\mathbf{S}_i^{\mathrm{A}} \cdot \mathbf{S}_j^{\mathrm{B}})(\mathbf{S}_k^{\mathrm{A}} \cdot \mathbf{S}_\ell^{\mathrm{B}}) + (\mathbf{S}_j^{\mathrm{B}} \cdot \mathbf{S}_k^{\mathrm{A}})(\mathbf{S}_\ell^{\mathrm{B}} \cdot \mathbf{S}_i^{\mathrm{A}}) - (\mathbf{S}_i^{\mathrm{A}} \cdot \mathbf{S}_k^{\mathrm{A}})(\mathbf{S}_\ell^{\mathrm{B}} \cdot \mathbf{S}_j^{\mathrm{B}}) \Big], \end{aligned} \tag{2}$$

where $j = i + \delta_x$, $k = i + \delta_x + \delta_y$, $\ell = i + \delta_y$ as shown in Fig. 1. Beside the directional anisotropy parameter $\zeta = J_1'/J_1$, the magnetic frustration between the NN and NNN spins $\eta = J_2/J_1$, and the cyclic four-spin exchange interaction term $\mu = KS^2/J_1$ we use $z = 2$ for the coordination number. This spin Hamiltonian is mapped onto an equivalent Hamiltonian of interacting bosons by expressing the spin operators in terms of bosonic creation and

annihilation operators $a^\dagger, a$ for "up" sites on sublattice A and $b^\dagger, b$ for "down" sites on sublattice B using the Dyson-Maleev representation

$$S^+_{Ai} = \sqrt{2S}\Big[a_i - \frac{a_i^\dagger a_i a_i}{(2S)}\Big],\ S^-_{Ai} = \sqrt{2S}a_i^\dagger,\ S^z_{Ai} = S - a_i^\dagger a_i, \tag{3a}$$

$$S^+_{Bj} = \sqrt{2S}\Big[b_j^\dagger - \frac{b_j^\dagger b_j^\dagger b_j}{(2S)}\Big],\ S^-_{Bj} = \sqrt{2S}b_j,\ S^z_{Bj} = -S + b_j^\dagger b_j. \tag{3b}$$

Substituting Eqs. (3) into (2) we expand the Hamiltonian perturbatively in powers of $1/S$ as

$$H = H_{-1} + H_0 + H_1 + H_2 + \cdots, \tag{4}$$

where H_m is of order $1/S^{m-1}$. Note that H_{-1} is just a number representing the classical energy. We do not discuss it further because it is irrelevant for the quantum fluctuations. Hence the $1/S$ expansion will be performed around the unperturbed Hamiltonian H_0 which is the zeroth order Hamiltonian in this sense. Relative to H_0 the terms H_1 and H_2 are first and second order terms, respectively.

Next the real space Hamiltonian is Fourier transformed to momentum space. Then we diagonalize the quadratic part H_0 by transforming the operators $a_\mathbf{k}$ and $b_\mathbf{k}$ to magnon operators $\alpha_\mathbf{k}$ and $\beta_\mathbf{k}$ using the usual Bogoliubov (BG) transformations

$$a_\mathbf{k}^\dagger = l_\mathbf{k}\alpha_\mathbf{k}^\dagger + m_\mathbf{k}\beta_{-\mathbf{k}}, \quad b_{-\mathbf{k}} = m_\mathbf{k}\alpha_\mathbf{k}^\dagger + l_\mathbf{k}\beta_{-\mathbf{k}}. \tag{5}$$

The coefficients $l_\mathbf{k}$ and $m_\mathbf{k}$ are defined as

$$l_\mathbf{k} = \Big[\frac{1+\epsilon_\mathbf{k}}{2\epsilon_\mathbf{k}}\Big]^{1/2},\ \ m_\mathbf{k} = -\mathrm{sgn}(\gamma_\mathbf{k})\Big[\frac{1-\epsilon_\mathbf{k}}{2\epsilon_\mathbf{k}}\Big]^{1/2} \equiv -x_\mathbf{k} l_\mathbf{k},\ \ x_\mathbf{k} = \mathrm{sgn}(\gamma_\mathbf{k})\Big[\frac{1-\epsilon_\mathbf{k}}{1+\epsilon_\mathbf{k}}\Big]^{1/2}, \tag{6}$$

with $\gamma_{kx} = \cos(k_x),\ \gamma_{ky} = \cos(k_y)$ and

$$\epsilon_\mathbf{k} = (1-\gamma_\mathbf{k}^2)^{1/2}, \tag{7a}$$

$$\gamma_\mathbf{k} = \frac{\gamma_{1\mathbf{k}}}{\kappa_\mathbf{k}}, \tag{7b}$$

$$\gamma_{1\mathbf{k}} = \frac{(1-4\mu)\gamma_{kx} + (\zeta - 4\mu)\gamma_{ky}}{1+\zeta-8\mu}, \tag{7c}$$

$$\gamma_{2\mathbf{k}} = \gamma_{kx}\gamma_{ky}, \tag{7d}$$

$$\kappa_\mathbf{k} = 1 - \frac{2(\eta - 2\mu)}{1+\zeta-8\mu}(1-\gamma_{2\mathbf{k}}). \tag{7e}$$

The function $\mathrm{sgn}(\gamma_\mathbf{k})$ keeps track of the sign of $\gamma_\mathbf{k}$ in the first Brillouin zone (BZ). After these transformations, the quadratic part of the Hamiltonian takes the form

$$H_0 = J_1 S z(1+\zeta-8\mu)\sum_\mathbf{k}\kappa_\mathbf{k}\left(\epsilon_\mathbf{k}-1\right) + J_1 S z(1+\zeta-8\mu)\sum_\mathbf{k}\kappa_\mathbf{k}\epsilon_\mathbf{k}\left(\alpha_\mathbf{k}^\dagger\alpha_\mathbf{k} + \beta_\mathbf{k}^\dagger\beta_\mathbf{k}\right). \tag{8}$$

The first term is the quantum zero-point energy and the second term represents the excitation energy of the magnons within linear spin-wave theory (LSWT).[16]

The part H_1 comprises $1/S$ contribution to the Hamiltonian. We follow the same procedure as described above. The resulting expression after transforming the bosonic operators to magnon operators is

$$\begin{aligned} H_1 &= \frac{J_1 Sz(1+\zeta-8\mu)}{2S}\sum_{\mathbf{k}}\Big[A_{\mathbf{k}}\left(\alpha^\dagger_{\mathbf{k}}\alpha_{\mathbf{k}}+\beta^\dagger_{\mathbf{k}}\beta_{\mathbf{k}}\right)+B_{\mathbf{k}}\left(\alpha^\dagger_{\mathbf{k}}\beta^\dagger_{-\mathbf{k}}+\beta_{-\mathbf{k}}\alpha_{\mathbf{k}}\right)\Big] \\ &- \frac{J_1 Sz(1+\zeta-8\mu)}{2SN}\sum_{1234}\delta_{\mathbf{G}}(1+2-3-4)l_1l_2l_3l_4\Big[V^{(1)}_{12;34}\alpha^\dagger_1\alpha^\dagger_2\alpha_3\alpha_4+2V^{(2)}_{12;34}\alpha^\dagger_1\beta_{-2}\alpha_3\alpha_4 \\ &+ 2V^{(3)}_{12;34}\alpha^\dagger_1\alpha^\dagger_2\beta^\dagger_{-3}\alpha_4+4V^{(4)}_{12;34}\alpha^\dagger_1\alpha_3\beta^\dagger_{-4}\beta_{-2}+2V^{(5)}_{12;34}\beta^\dagger_{-4}\alpha_3\beta_{-2}\beta_{-1}+2V^{(6)}_{12;34}\beta^\dagger_{-4}\beta^\dagger_{-3}\alpha^\dagger_2\beta_{-1} \\ &+ V^{(7)}_{12;34}\alpha^\dagger_1\alpha^\dagger_2\beta^\dagger_{-3}\beta^\dagger_{-4}+V^{(8)}_{12;34}\beta_{-1}\beta_{-2}\alpha_3\alpha_4+V^{(9)}_{12;34}\beta^\dagger_{-4}\beta^\dagger_{-3}\beta_{-2}\beta_{-1}\Big]. \end{aligned} \tag{9}$$

In the above equation momenta $\mathbf{k}_1, \mathbf{k}_2, \mathbf{k}_3, \mathbf{k}_4$ are abbreviated as 1, 2, 3, and 4. The first term in Eq. (9) is obtained by normal ordering the products of four boson operators with respect to creation and annihilation in the magnon operators, i.e., magnon creation operators appear always to the left of magnon annihilation operators. The coefficients $A_{\mathbf{k}}$ and $B_{\mathbf{k}}$ read

$$A_{\mathbf{k}} = A_1\frac{1}{\kappa_{\mathbf{k}}\epsilon_{\mathbf{k}}}\Big[\kappa_{\mathbf{k}}-\gamma^2_{1\mathbf{k}}\Big]+A_2\frac{1}{\epsilon_{\mathbf{k}}}\Big[1-\gamma_{2\mathbf{k}}\Big]+A_3\frac{1}{\epsilon_{\mathbf{k}}}\Big[(1+\gamma_{2\mathbf{k}})-\gamma_{\mathbf{k}}(\gamma_{kx}+\gamma_{ky})\Big], \tag{10a}$$

$$B_{\mathbf{k}} = B_1\frac{1}{\kappa_{\mathbf{k}}\epsilon_{\mathbf{k}}}\gamma_{1\mathbf{k}}\Big[1-\gamma_{2\mathbf{k}}\Big]+A_3\frac{1}{\epsilon_{\mathbf{k}}}\Big[(\gamma_{kx}+\gamma_{ky})-\gamma_{\mathbf{k}}(1+\gamma_{2\mathbf{k}})\Big], \tag{10b}$$

where the shorthands

$$A_1 = \Big(\frac{2}{N}\Big)\sum_{\mathbf{p}}\frac{1}{\epsilon_{\mathbf{p}}}\Big[\gamma_{\mathbf{p}}\gamma_{1\mathbf{p}}+\epsilon_{\mathbf{p}}-1\Big], \tag{11a}$$

$$A_2 = \frac{2(\eta-4\mu)}{1+\zeta-8\mu}\Big(\frac{2}{N}\Big)\sum_{\mathbf{p}}\frac{1}{\epsilon_{\mathbf{p}}}\Big[1-\epsilon_{\mathbf{p}}-\gamma_{2\mathbf{p}}\Big], \tag{11b}$$

$$A_3 = \frac{4\mu}{1+\zeta-8\mu}\Big(\frac{2}{N}\Big)\sum_{\mathbf{p}}\frac{2}{\epsilon_{\mathbf{p}}}\Big[1-\epsilon_{\mathbf{p}}+\gamma_{2\mathbf{p}}-\gamma_{\mathbf{p}}(\gamma_{px}+\gamma_{py})\Big], \tag{11c}$$

$$B_1 = \frac{2(\eta-2\mu)}{1+\zeta-8\mu}\Big(\frac{2}{N}\Big)\sum_{\mathbf{p}}\frac{1}{\epsilon_{\mathbf{p}}}\Big[\gamma_{2\mathbf{p}}-\gamma_{\mathbf{p}}\gamma_{1\mathbf{p}}\Big] \tag{11d}$$

are used.

The second term in Eq. (9) represents scattering between spin-waves where the delta function $\delta_{\mathbf{G}}(1+2-3-4)$ ensures that the momentum is conserved within a reciprocal lattice vector $\mathbf{G}$. Explicit forms of the vertex factors $V^{i=2,3,5,7,8}_{1234}$ are given in Appendix B.

The second order term, H_2 is composed of six-boson operators and is only present when $\mu \neq 0$. Before the Fourier and BG transformations H_2 is of the following form

$$\begin{aligned} H_2 \;=\; & -\frac{8\mu S}{(2S)^2}\sum_i \Big[(a_i^\dagger a_i + b_j^\dagger b_j + a_i b_j + a_i^\dagger b_j^\dagger)(a_k^\dagger a_k b_\ell^\dagger b_\ell + \frac{1}{2}a_k^\dagger a_k a_k b_\ell + \frac{1}{2}a_k^\dagger b_\ell^\dagger b_\ell^\dagger b_\ell) \\ & + (a_k^\dagger a_k + b_j^\dagger b_j + a_k b_j + a_k^\dagger b_j^\dagger)(a_i^\dagger a_i b_\ell^\dagger b_\ell + \frac{1}{2}a_i^\dagger a_i a_i b_\ell + \frac{1}{2}a_i^\dagger b_\ell^\dagger b_\ell^\dagger b_\ell) \\ & + (a_i^\dagger a_i b_j^\dagger b_j + \frac{1}{2}a_i^\dagger a_i a_i b_j + \frac{1}{2}a_i^\dagger b_j^\dagger b_j^\dagger b_j)(a_k^\dagger a_k + b_\ell^\dagger b_\ell + a_k b_\ell + a_k^\dagger b_\ell^\dagger) \\ & + (a_k^\dagger a_k b_j^\dagger b_j + \frac{1}{2}a_k^\dagger a_k a_k b_j + \frac{1}{2}a_k^\dagger b_j^\dagger b_j^\dagger b_j)(a_i^\dagger a_i + b_\ell^\dagger b_\ell + a_i b_\ell + a_i^\dagger b_\ell^\dagger) \\ & - (a_i^\dagger a_i + a_k^\dagger a_k - a_i a_k^\dagger - a_i^\dagger a_k)(b_j^\dagger b_j b_\ell^\dagger b_\ell - \frac{1}{2}b_j^\dagger b_j^\dagger b_j b_\ell - \frac{1}{2}b_j b_\ell^\dagger b_\ell^\dagger b_\ell) \\ & - (a_i^\dagger a_i a_k^\dagger a_k - \frac{1}{2}a_i^\dagger a_i a_i a_k^\dagger - \frac{1}{2}a_i^\dagger a_k^\dagger a_k a_k)(b_j^\dagger b_j + b_\ell^\dagger b_\ell - b_j b_\ell^\dagger - b_j^\dagger b_\ell)\Big]. \end{aligned} \tag{12}$$

After Fourier and BG transformations to magnon operators $\alpha_{\mathbf{k}}, \beta_{\mathbf{k}}$ the Hamiltonian in normal-ordered form reduces to

$$H_2 = -\frac{4\mu z S}{(2S)^2}\sum_{\mathbf{k}}\Big[\mathcal{C}_{1\mathbf{k}}\left(\alpha_{\mathbf{k}}^\dagger\alpha_{\mathbf{k}} + \beta_{\mathbf{k}}^\dagger\beta_{\mathbf{k}}\right) + \mathcal{C}_{2\mathbf{k}}\left(\alpha_{\mathbf{k}}^\dagger\beta_{-\mathbf{k}}^\dagger + \beta_{-\mathbf{k}}\alpha_{\mathbf{k}}\right) + ...\Big]. \tag{13}$$

The dotted terms contribute only to higher than second order corrections and are thus omitted in our calculations. The coefficients $C_{1\mathbf{k}}$ and $C_{2\mathbf{k}}$ are given in Appendix C.

The quasiparticle energy $\tilde{E}_{\mathbf{k}}^{\mathrm{AF}}$ for magnon excitations, measured in units of $J_1 S z(1+\zeta-8\mu)$ up to second order in $1/S$ is given as

$$\tilde{E}_{\mathbf{k}}^{\mathrm{AF}} = E_{\mathbf{k}} + \frac{1}{(2S)}A_{\mathbf{k}} + \frac{1}{(2S)^2}\Big[\Sigma_{\alpha\alpha}^{(2)}(\mathbf{k}, E_{\mathbf{k}}) - \frac{B_{\mathbf{k}}^2}{2E_{\mathbf{k}}}\Big]. \tag{14}$$

Expressions for the magnon Green's functions and self-energies are given in Appendix A. The dynamic contributions to the second order self-energies $\Sigma^{(2)}$ are second order in the vertex factors $V^{(j)}$. These are the contributions which are missed by self-consistent spin-wave theory.

The sublattice magnetization M_{AF} for the A sublattice can be expressed as

$$M_{\mathrm{AF}} = S - \langle a_i^\dagger a_i\rangle = S - \Delta S + \frac{M_1}{(2S)} + \frac{M_2}{(2S)^2}, \tag{15}$$

where

$$\Delta S = \frac{2}{N}\sum_{\mathbf{k}}\frac{1}{2\epsilon_{\mathbf{k}}} - \frac{1}{2}, \tag{16a}$$

$$M_1 = \frac{2}{N}\sum_{\mathbf{k}}\frac{l_{\mathbf{k}}m_{\mathbf{k}}B_{\mathbf{k}}}{E_{\mathbf{k}}}, \tag{16b}$$

$$\begin{aligned} M_2 = \frac{2}{N}\sum_{\mathbf{k}}\Big\{ & -(l_{\mathbf{k}}^2+m_{\mathbf{k}}^2)\frac{B_{\mathbf{k}}^2}{4E_{\mathbf{k}}^2} + \frac{l_{\mathbf{k}}m_{\mathbf{k}}}{E_{\mathbf{k}}}\Sigma^{(2)}_{\alpha\beta}(\mathbf{k},-E_{\mathbf{k}}) \\ & - \Big(\frac{2}{N}\Big)^2\sum_{\mathbf{pq}} 2l_{\mathbf{k}}^2 l_{\mathbf{p}}^2 l_{\mathbf{q}}^2 l_{\mathbf{k+p-q}}^2 \Big[\frac{(l_{\mathbf{k}}^2+m_{\mathbf{k}}^2)V^{(7)}_{\mathbf{k},\mathbf{p},\mathbf{q},[\mathbf{k+p-q}]}V^{(8)}_{[\mathbf{k+p-q}],\mathbf{q},\mathbf{p},\mathbf{k}}}{(E_{\mathbf{k}}+E_{\mathbf{p}}+E_{\mathbf{q}}+E_{\mathbf{k+p-q}})^2} \\ & + \frac{2l_{\mathbf{k}}m_{\mathbf{k}}V^{(7)}_{\mathbf{k},\mathbf{p},\mathbf{q},[\mathbf{k+p-q}]}V^{(5)}_{[\mathbf{k+p-q}],\mathbf{q},\mathbf{p},\mathbf{k}}}{E_{\mathbf{k}}^2-(E_{\mathbf{p}}+E_{\mathbf{q}}+E_{\mathbf{k+p-q}})^2}.\Big]\Big\} \end{aligned} \tag{16c}$$

The zeroth-order term ΔS corresponds to the reduction of magnetization within LSWT, M_1 term corresponds to the first-order $1/S$ correction, and M_2 is the second-order correction. Again, the parts which are second order in the vertex factors are not captured by self-consistent spin-wave theory.

III. RESULTS

1. Spin-Wave Energy

We obtain the spin-wave energy $2J_1S(1+\zeta-8\mu)\tilde{E}^{\rm AF}_{\mathbf{k}}$ for $S=1/2$ as a function of momenta (k_x,k_y) for several values of ζ,η, and μ by evaluating Eq. (14) in the first BZ. For the numerical summation we divide the first BZ in a mesh of N_L^2 points with $N_L=48$ and then the contributions from all the points are summed up to evaluate the third term in Eq. (14). In the Dyson-Maleev formalism, no cancellation of divergences occurs so that the convergence of the numerical results for $N_L\to\infty$ is very good. This is a crucial advantage over the use of the Holstein-Primakov representation. We estimate that the results for $N_L=48$ will not change more than in the third digit if N_L is chosen larger.

Figure 2 shows a comparison between the results from LSWT (long-dashed lines), first-order (dot-dashed lines) and second-order corrections (solid lines) to the spin-wave energy spectrum for isotropic coupling ($\zeta=1$) for two choices of frustration and and ring exchange. For the moderate value $\mu=0.025$ corresponding to $2K/J_1=0.2$ the $1/S$ correction is substantial while the $1/S^2$ correction is fairly small. This is very similar to the corrections

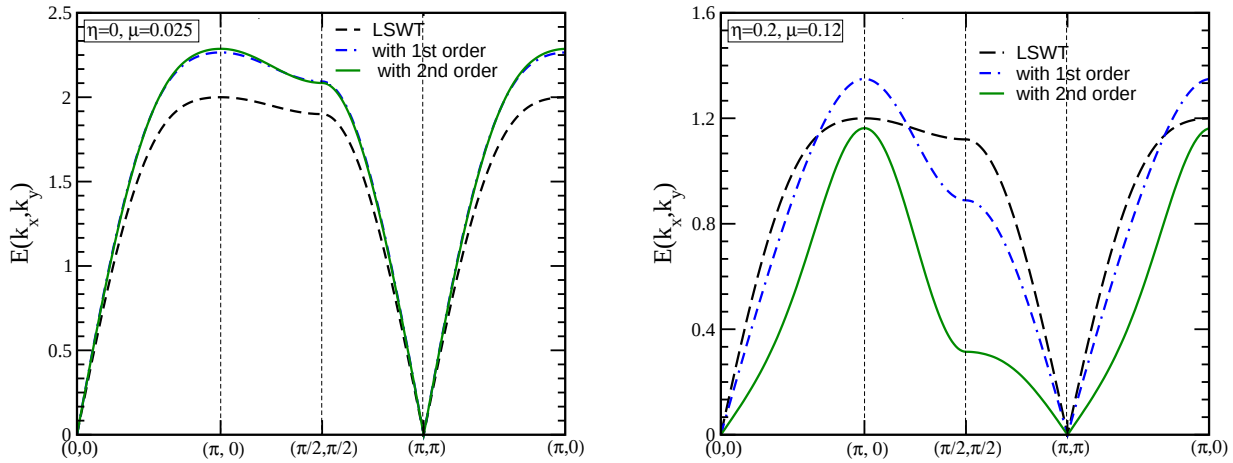

FIG. 2: (Color online) Spin-wave energy $E^{\rm AF}_{\mathbf{k}}/J_1$ obtained from LSWT (long-dashed lines), with $1/S$ (dot-dashed lines) and with $1/S^2$ corrections (solid lines) for the Néel-ordered phase. We have chosen spatially isotropic coupling $\zeta = 1$. In the left panel we show the corrections for relative frustration $\eta = 0$ and ring exchange $\mu = 0.025$; in the right panel we show them for frustration $\eta = 0.2$ and ring exchange $\mu = 0.12$. In the latter case, the $1/S^2$ terms in the Hamiltonian provide significant corrections to both the LSWT and $1/S$ results.

for the NN Heisenberg model at $\mu = 0$.[58–60,67–69] The right panel of Fig. 2 tells quite a different story. For substantial ring exchange the quantum corrections are very large and cannot be ignored. We point out that this is not due to the frustration alone as can be seen by inspecting the results for substantial values of η, but without ring exchange $\mu = 0$, in Ref. 60. The $1/S^2$ corrections for $\mu = 0$ are as small as they are for the NN Heisenberg model, in contrast to the result in the right panel of Fig. 2.

In the panels of Fig. 3 the evolution of the spin-wave energy spectrum including corrections up to second-order for various values of ζ, η and μ are shown. The spin-wave dispersions for the couplings $\zeta = 1$ and $\zeta = 0.4$ at $\mu = 0$ were reported earlier using the Holstein-Primakov representation.[60] The results from the Dyson-Maleev and from the Holstein-Primakov representation coincide as it has to be for physically observable results of a systematic expansion in a small parameter.

For $\mu = 0$ and $\eta = 0$, the energy at $(\pi/2, \pi/2)$ is larger than the energy at $(\pi, 0)$, cf. upper left panel in Fig. 3. This dip of the dispersion at $(\pi, 0)$ has been first computed by high-order series expansion (HSE) around the Ising limit[70,71] and was confirmed by quantum Monte Carlo calculation (QMC).[72] HSE and QMC find that the dip is about 9% deep, i.e.,

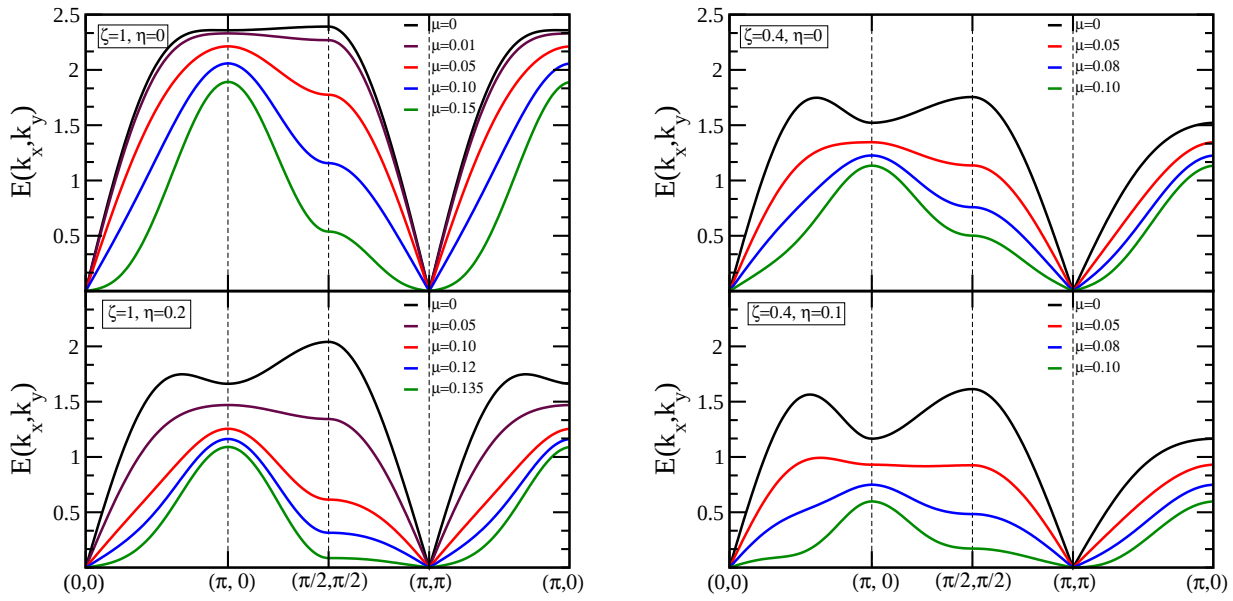

FIG. 3: (Color online) The effect of μ on the spin-wave energy $E^{\rm AF}_{\mathbf{k}}/J_1$ for the Néel-ordered phase with $1/S^2$ corrections is shown for two values of $\eta = 0, 0.2$ and $\zeta = 1$.

$[E((\pi/2,\pi/2)) - E((\pi,0))]/E((\pi/2,\pi/2)) \approx 0.09$. Experimentally, the dip is found to be about 7% in compounds in which no couplings beyond J_1 are thought to play a role, in reasonable agreement with HSE and QMC.[4,5]

In contrast, LSWT and order $1/S$ do not find a dip at all. In order $1/S^2$, it is present but as small as 1.4% and in order $1/S^3$ it takes the value of 3.2%.[69] Thus one must be aware that the data in Fig. 3 does not capture all aspects of the dispersion between $(\pi, 0)$ and $(\pi/2, \pi/2)$. But in the remaining BZ the significance of corrections of third order and higher is rather small and the agreement with the series expansion results very good.

Having the above minor caveat in mind, we discuss the much stronger influence of frustration and of ring exchange in the following. Increasing the value of μ to positive values the energy at $(\pi/2, \pi/2)$ decreases more strongly than the one at $(\pi, 0)$, see left panels of Fig. 3. Hence, beyond some finite value of four-spin ring exchange there is a dip from $(\pi, 0)$ to $(\pi/2, \pi/2)$. This agrees qualitatively with experimental findings[1,2], which see a 13% dip, and with an analysis based on self-consistent spin-wave theory.[28] Even larger values of μ will lead to a complete softening of the magnon mode at $(\pi/2, \pi/2)$. This indicates a competition between an ordered orthogonal state at modulation $(\pi/2, \pi/2)$ and the ordered Néel state at (π, π) upon increasing μ.

Another important issue is the effect of finite frustration $\eta > 0$ which has been investigated before without ring exchange.[59,60] Indeed, finite frustration induces a significant dip at $(\pi, 0)$ relative to $(\pi/2, \pi/2)$, i.e., $E((\pi, 0)) < E((\pi/2, \pi/2))$, so that frustration pushes the system into the opposite direction as does the ring exchange. But in the presence of *substantial* ring exchange the effect is reversed: Comparing the upper and lower left panels in Fig. 3 and inspecting Fig. 4 we see that increasing frustration supports the tendency to soften the mode at $(\pi/2, \pi/2)$ which will eventually destabilize the Néel order.

Spatial anisotropy, see right panel in Fig. 3, does not alter this picture qualitatively. A strong anisotropy $\zeta < 1$ seems to support the tendency to mode softening and the concomitant destabilization of the Néel order.

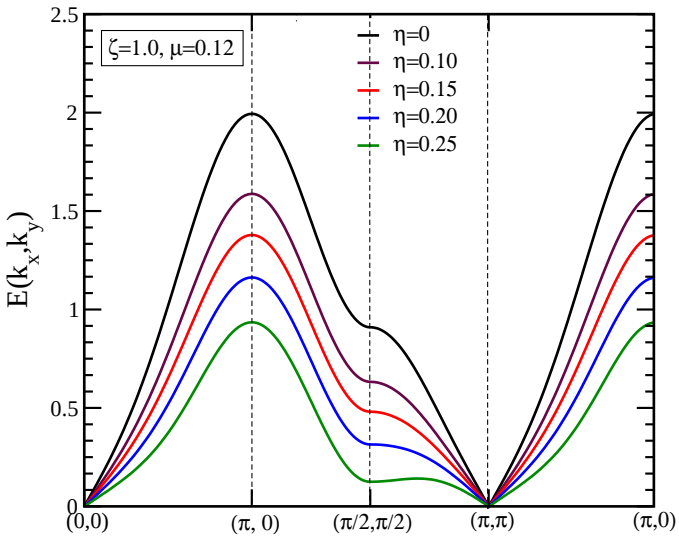

FIG. 4: (Color online) Spin-wave energy $E^{\mathrm{AF}}_{\mathbf{k}}/J_1$ including $1/S^2$ corrections for $\zeta = 1, \mu = 0.12$ for various values of η.

2. *Quantitative Analysis of the Inelastic Neutron Scattering Data*

We use our model to quantitatively analyse the experimental data obtained in Ref. 2 by inelastic neutron scattering for La_2CuO_4. We disregard any spatial anisotropy because La_2CuO_4 is tetragonal so that we set $\zeta = 1$. The experimental data displays a significant dip at $(\pi/2, \pi/2)$ relative to the energy at $(\pi, 0)$. This points toward a sizable four-spin ring exchange[1,28].

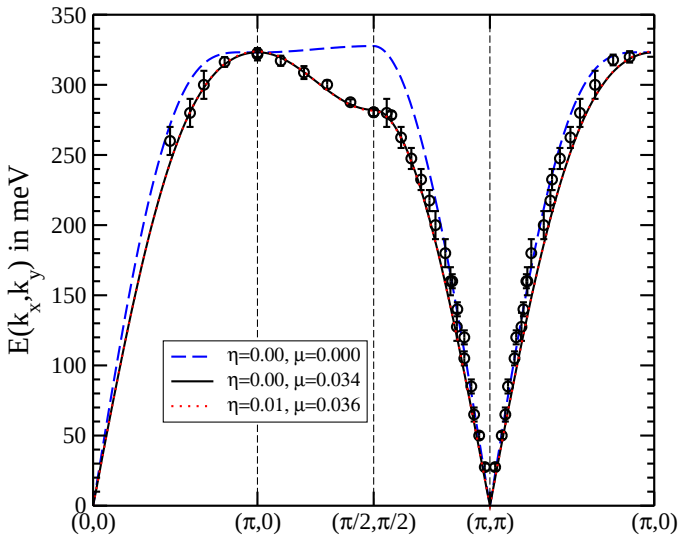

FIG. 5: (Color online) Comparison of the measured spin-wave energy $E_{\mathbf{k}}^{\mathrm{AF}}$ as obtained by inelastic neutron scattering in La_2CuO_4 with the theoretical results including $1/S^2$ corrections for the spatially isotropic model ($\zeta = 1$) for $N_L = 24$. For given moderate values η of relative frustration a value μ of the four-spin ring exchange can be found such that the dispersions match the experimental data.

Our findings are shown in Fig. 5. They strikingly confirm that substantial values of μ are needed to explain the observed energy dip at $(\pi/2, \pi/2)$. For instance, for $\eta = 0$ one needs $\mu = 0.034$, and $J_1 = 143$ meV; for $\eta = 0.01$ $\mu = 0.036$, and $J_1 = 146$ meV; for $\eta = 0.02$ $\mu = 0.0375$, and $J_1 = 148$ meV (not shown). Even for $\eta = 0.10$ the parameters $\mu = 0.046$, and $J_1 = 174$ meV yield a theoretical dispersion which is indistinguishable from those displayed in Fig. 5. Note that the agreement of the steeply rising parts of the dispersion is not completely perfect because the theoretical curves remain a bit below the experimental data points.

We conclude that from the experimental data for the spin-wave energies the relative frustration and the relative ring exchange cannot both be determined independently. Based on the results of systematic derivations of extended Heisenberg models for the cuprates starting from microscopic Hubbard models[19,23,24] we stick to small values of frustration $\eta \approx 0.01$. According to our fits this implies $x_{\mathrm{ring}} = 2K/J_1 = 8\mu = 0.29$. This relative four-spin ring exchange is slightly larger than we would expect from the systematic derivations.[19,23,24] It is also slightly larger than the value 0.24 found in the analysis by self-consistent spin-wave

theory.[28]

On the one hand, the agreement is good in view of the remaining uncertainty in the description of the spin-wave energies at the zone boundary, see our discussion above. On the other hand, a further improved theoretical treatment of spin-waves is desirable.

3. Sublattice Magnetization and the Phase Diagram

We calculate the sublattice magnetization $M_{\rm AF}$ from Eq. (15) by numerically evaluating Eqs. (16a)–(16c) with $\zeta = 1$ and 0.8 and for $\mu = 0, 0.12$ and 0.22. Especially to obtain the second order correction term M_2 we sum up the values of $N_L^2/4$ points of $\mathbf{k}$ in a quarter of the first BZ and N_L^2 points of $\mathbf{p}$ and $\mathbf{q}$ in the first BZ, with $N_L = 36$ sites along one axis.

Figure 6 shows the sublattice magnetization with increase in the frustration parameter $\eta = J_2/J_1$ for the isotropic case $\zeta = J_1'/J_1 = 1$ for three different values of plaquette ring exchange coupling $\mu = KS^2/J_1 = 0, 0.12$, and 0.22. For each case, three different curves are plotted: The long-dashed lines represent the LSWT prediction, the dotted lines include the first-order $(1/S)$ correction to the LSWT results, and the solid lines include corrections up to second-order $(1/S^2)$. Upon increasing frustration the dotted curves of the first-order corrections diverge. However, $1/S^2$ corrections (M_2) significantly increase with frustration and stabilize the apparent divergence of the magnetization. We find that the magnetization with second-order corrections decreases steadily at first with increase in η and then sharply drops to zero at a critical value of $\eta = \eta_c$. Assuming that the Néel phase loses its stability continuously, η_c marks the quantum critical point at which the AF order is destroyed and the system enters into another state characterized by other types of order. The precise order of the phase transition and the nature of the subsequent phase is still matter of intense debate.[63–65].

Without four-spin ring exchange, i.e., $\mu = 0$, $M_{\rm AF}$ with second-order corrections begins from 0.307 at $\eta = 0$ and decreases upon rising frustration till $\eta \approx 0.32$. Finally it vanishes at $\eta_{c1} \approx 0.411$. For this case, we reproduce the magnetization plot obtained in Ref. 60 using a similar perturbative $1/S$ expansion based on the Holstein-Primakov representation. The LSWT prediction for the critical point is lower at ≈ 0.38. With increase in the four-spin ring exchange μ the values of the magnetization at $\eta = 0$ increase. For example, we find $M_{\rm AF}(\eta = 0, \mu = 0.12) \approx 0.458$ and $M_{\rm AF}(\eta = 0, \mu = 0.22) \approx 0.524$. These numbers are

significantly larger than the predictions from LSWT which are 0.381 and 0.466, respectively. We conclude that without NNN frustration ($\eta = 0$) the pure four-spin coupling μ favors the Néel order. This is in qualitative accord with the observation that the spin gap of the disordered paramagnetic phase of spin ladders is reduced on increasing four-spin coupling μ.[12,30,32,33] Thus finite four-spin coupling pushes spin ladders closer to a gapless phase which is likely to display quasi-long range order with powerlaw correlations.

We observe that first and second order corrections provide significant contributions to the entire magnetization curves. For small μ, the corrections M_2 start from a small positive value and then switch sign and become negative with increase in η. However, for large μ, say $\mu = 0.22$ M_2, corrections are negative throughout.

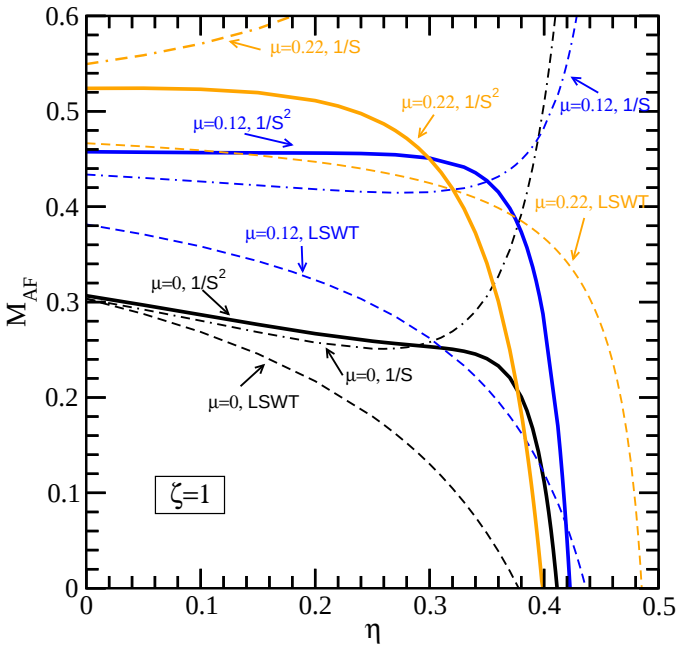

FIG. 6: (Color online) The sublattice magnetization $M_{\rm AF}$ is plotted for $\zeta = 1$ and for three different values of $\mu = 0$ (black), 0.12 (blue/dark gray), 0.22 (orange/light gray) as a function of the relative magnetic frustration η. For all three cases, results from linear spin-wave theory (dashed lines), with $1/S$ (dot-dashed lines), and with $1/S^2$ corrections (solid lines) are shown. Magnetization curves with $1/S$ corrections alone diverge in all cases. However, $1/S^2$ corrections compensate the divergence and the magnetization curves steadily decrease to zero at critical values η_c We find $\eta_c = 0.411$ ($\mu = 0$), 0.423 ($\mu = 0.12$), and 0.399 ($\mu = 0.22$).

Another interesting feature portrayed in Fig. 6 is the change in the critical value of η

with μ. For $\mu = 0$ the magnetization vanishes at the critical value of frustration $\eta_c \approx 0.411$. With increase in μ, the value of η_c increases initially till a turning value of $\mu = \mu_t \approx 0.12$ is reached beyond which η_c decreases again. For example, $\eta_c \approx 0.423$ for $\mu = 0.12$, but $\eta_c \approx 0.399$ for $\mu = 0.22$. This implies that the four-spin ring exchange interaction favors the Néel order and thus extends the AF region only for small values. Beyond the turning value $\mu = \mu_t$ is reached the ring exchange coupling destabilizes the Néel phase. This is shown in the η_c-μ phase diagram in Fig. 7.

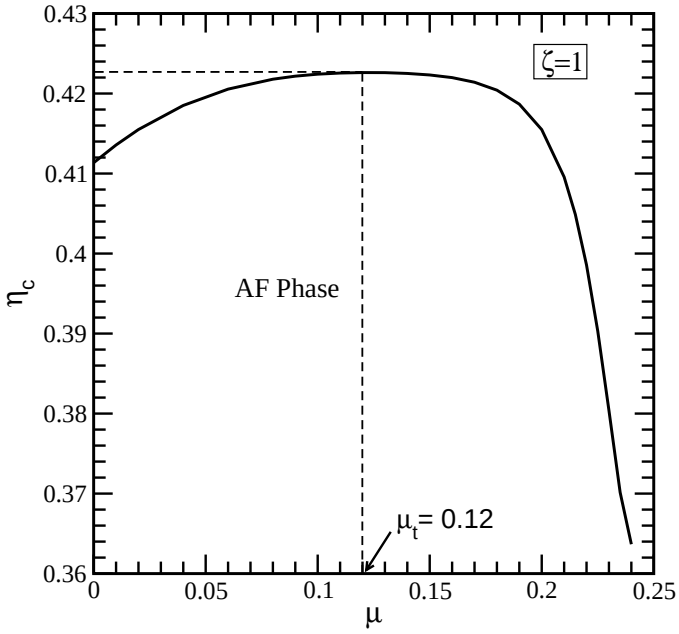

FIG. 7: (Color online) η_c-μ phase diagram for $\zeta = 1$. With increase in μ, η_c increases up to a maximum value 0.423 at $\mu = \mu_t \approx 0.12$ and then sharply decreases. This shows that the ring exchange coupling μ initially favors the Néel ordering of the NN spins till the turning value μ_t is reached. For $\mu > \mu_t$, the four-spin coupling enhances destabilizes the Néel order.

Next we study the influence of directional anisotropy between the horizontal and vertical NN couplings implying $\zeta < 1$. This spatial anisotropy does not lead to frustration, but it weakens the NN coupling because the vertical NN coupling is lowered. Hence we expect a qualitatively similar behavior as before, but at lower values of η and μ. This expectation is confirmed by the following results.

Figure 8 shows the magnetization upon increasing η for the spatially anisotropic case. We choose $\zeta = 0.4$ with the three values of ring exchange coupling $\mu = 0, 0.08$, and 0.13. Here the values of the magnetization without NNN frustration are $M_{\rm AF}(\eta = 0, \mu = 0.08) \approx 0.40$

and $M_{\rm AF}(\eta = 0, \mu = 0.13) \approx 0.438$. Again these numbers are again larger than the LSWT values which are 0.350 and 0.406, respectively.

It is interesting to observe that with increase in η the magnetization with just $1/S$ corrections (dotted curves) diverge except for the case when $\mu = 0.13$. We find that this divergence ceases to occur for $\mu \gtrapprox 0.10$. As before, $1/S^2$ corrections significantly modify the magnetization curves. The critical values of η at which the Néel phase is unstable are 0.176, 0.191, and 0.15 for $\mu = 0, 0.08$ and 0.13, respectively. The LSWT predictions for these three cases are 0.172, 0.188, and 0.194, respectively. Notice that the LSWT prediction $\eta_c = 0.194$ for $\mu = 0.13$ is larger than the value $\eta_c = 0.15$ obtained including first and second order corrections.

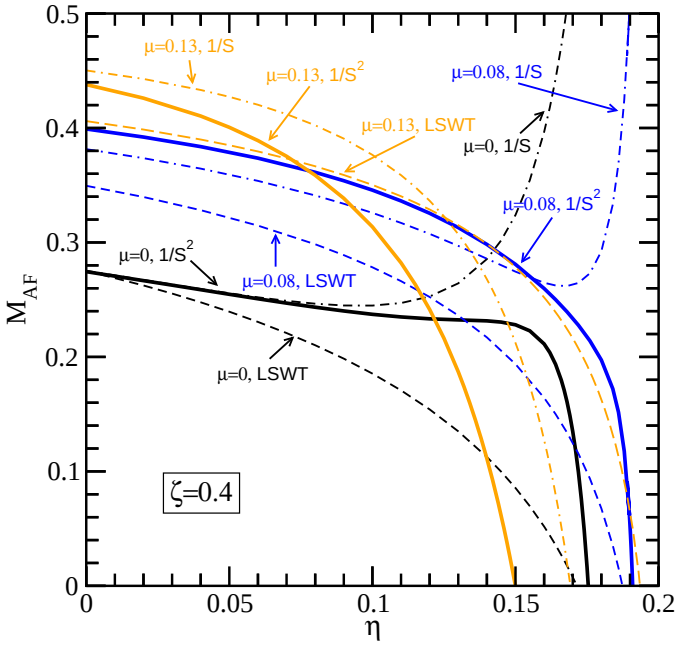

FIG. 8: (Color online) Sublattice magnetization $M_{\rm AF}$ with spatial anisotropy $\zeta = 0.4$ between the vertical and the horizontal NN couplings for three values of $\mu = 0$ (black), 0.08 (blue/dark gray), 0.13 (orange/light gray) as a function of frustration η. For all three cases, results from LSWT (dashed lines), with $1/S$ (dot-dashed lines), and with $1/S^2$ corrections (solid lines) are shown. $M_{\rm AF}$ with $1/S$ corrections alone diverge for $\mu = 0$ and 0.08, but not for $\mu = 0.13$ where it converges, cf. main text

.

It is worth exploring the influence of the spatial anisotropy ζ on the η_c-μ phase diagram.

This is done in the panels of Fig. 9 for $\zeta = 0.4$ and 0.2. The results are qualitatively similar to those for $\zeta = 1$ in Fig. 7, but at lower values of η and μ as we expected. The Néel phase is stabilized by small values of μ. But beyond the turning values μ_t the four-spin ring exchange starts to reduce the parameter region of the Néel phase.

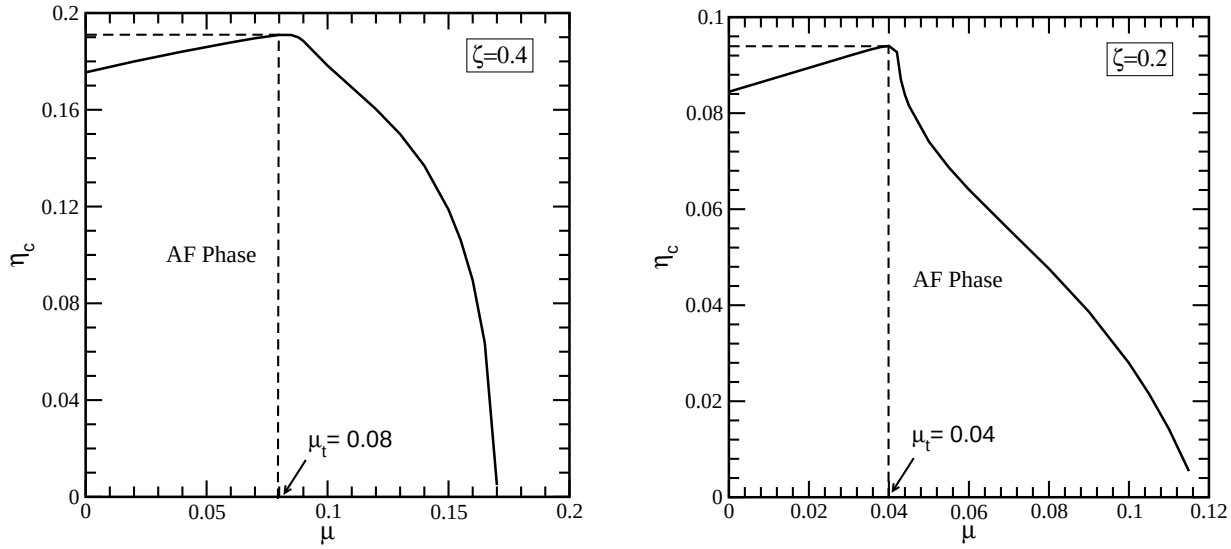

FIG. 9: (Color online) η_c-μ phase diagram for $\zeta = 0.4$ (left panel) and 0.2 (right panel), to be compared with the phase diagram for the spatially isotropic case $\zeta = 1$ in Fig. 7

.

IV. CONCLUSIONS

For $S = 1/2$ Heisenberg the four-spin ring exchange coupling on plaquettes is the next important interaction after the nearest-neighbor exchange. In this work we have investigated its influence on the zero temperature magnetic phase diagram of a spatially anisotropic and frustrated Heisenberg antiferromagnet on the square lattice.

In particular, we studied higher-order quantum effects in a systematic perturbative spin-wave expansion in the inverse spin S. We have calculated the spin-wave energy and the magnetization up to and including the second-order corrections. They contribute significantly to the shape of the magnetic phase diagram, especially as the frustration between the next-nearest neighbor spins increases. The obtained magnetic phase diagram shows that the four-spin ring exchange coupling initially favors the Néel order until a specific turning value is reached. Beyond this values a further increase in the ring exchange coupling increases

the frustration in the system and reduces the parameter region in which the Néel order represents the stable ground state.

Moreover, we analyzed the available neutron scattering data and found that a ring exchange coupling $2K$ of about 27% to 29% of the nearest-neighbor exchange is required to explain the data. The additional determination of the relative frustration in a three-parameter fit is not possible because the dispersions for various triples of nearest-neighbor exchange, frustration, and four-spin ring exchange are indistinguishable if the energies at $(\pi, 0)$ and $(\pi/2, \pi/2)$ are matched.

V. ACKNOWLEDGMENT

We are grateful to R. Coldea and S. Hayden for providing the inelastic neutron scattering data. The authors acknowledge the Texas Advanced Computing Center (TACC) at The University of Texas at Austin for providing HPC resources that have contributed to the research results reported within this paper.

Appendix A: Green's functions and Self-energies

The time-ordered magnon Green's functions are defined as

$$G_{\alpha\alpha}(\mathbf{k},t) = -i\langle T(\alpha_{\mathbf{k}}(t)\alpha^{\dagger}_{\mathbf{k}}(0))\rangle, \quad G_{\beta\beta}(\mathbf{k},t) = -i\langle T(\beta^{\dagger}_{-\mathbf{k}}(t)\beta_{-\mathbf{k}}(0))\rangle, \tag{A1a}$$

$$G_{\alpha\beta}(\mathbf{k},t) = -i\langle T(\alpha_{\mathbf{k}}(t)\beta_{-\mathbf{k}}(0))\rangle, \quad G_{\beta\alpha}(\mathbf{k},t) = -i\langle T(\beta^{\dagger}_{-\mathbf{k}}(t)\alpha^{\dagger}_{\mathbf{k}}(0))\rangle, \tag{A1b}$$

Considering H_0 as the unperturbed Hamiltonian the Fourier transformed unperturbed propagators are

$$G^0_{\alpha\alpha}(\mathbf{k},\omega) = \frac{1}{\omega - E_k + i\delta}, \quad G^0_{\beta\beta}(\mathbf{k},\omega) = \frac{1}{-\omega - E_k + i\delta}, \tag{A2a}$$

$$G^0_{\alpha\beta}(\mathbf{k},\omega) = G^0_{\beta\alpha}(\mathbf{k},\omega) = 0, \tag{A2b}$$

with $\delta \to 0+$. The spin-wave energy $E_{\mathbf{k}} = \kappa_{\mathbf{k}}\epsilon_{\mathbf{k}}$ is measured in units of $J_1 Sz(1 + \zeta - 8\mu)$. The graphical representations of the Green functions are shown in Fig. 10(a). Note the differing convention for the arrows which help to represent the conservation of the total S_z component in the diagrams efficiently, see Fig. 10.

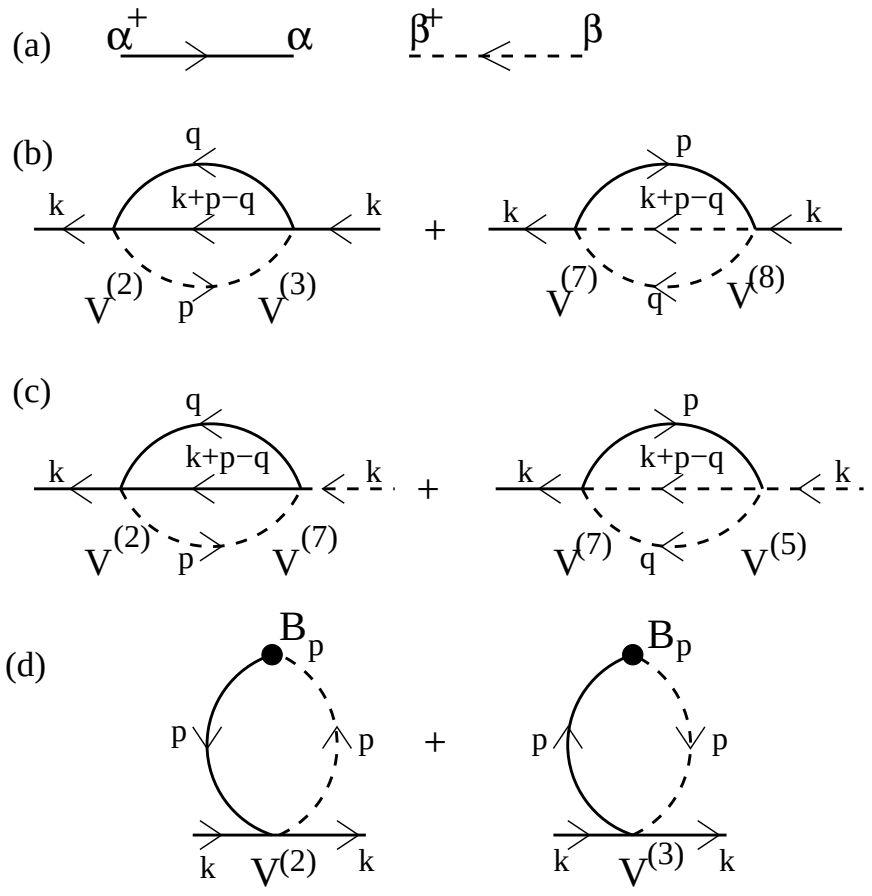

FIG. 10: (a) The solid and the dashed lines correspond to the α and β propagators. Second-order diagrams for the self-energies $\Sigma^{(2)}_{\alpha\alpha}(\mathbf{k},\omega)$ and $\Sigma^{(2)}_{\alpha\beta}(\mathbf{k},\omega)$ are shown in (b) and (c). The diagrams in (d) contribute only to $\Sigma^{(2)}_{\alpha\alpha}(\mathbf{k},\omega)$. $V^{(2)}, V^{(3)}, V^{(5)}, V^{(7)}, V^{(8)}$ are the vertex factors, see main text. Note that at each vertex two arrows enter the vertex and two leave it which reflects the conservation of the total S_z component.

The full propagators $G_{ij}(\mathbf{k},\omega)$ satisfy the matrix Dyson equation

$$G_{ij}(\mathbf{k},\omega) = G^0_{ij}(\mathbf{k},\omega) + \sum_{mn} G^0_{im}(\mathbf{k},\omega)\Sigma_{mn}(\mathbf{k},\omega)G_{nj}(\mathbf{k},\omega), \tag{A3}$$

where the self-energy $\Sigma_{ij}(\mathbf{k})$ can be expressed in powers of $1/(2S)$ as

$$\Sigma_{ij}(\mathbf{k},\omega) = \frac{1}{(2S)}\Sigma^{(1)}_{ij}(\mathbf{k},\omega) + \frac{1}{(2S)^2}\Sigma^{(2)}_{ij}(\mathbf{k},\omega) + \ldots. \tag{A4}$$

The first-order self-energy terms read

$$\Sigma^{(1)}_{\alpha\alpha}(\mathbf{k},\omega) \;=\; \Sigma^{(1)}_{\beta\beta}(\mathbf{k},\omega) = A_{\mathbf{k}}, \tag{A5a}$$

$$\Sigma^{(1)}_{\alpha\beta}(\mathbf{k},\omega) \;=\; \Sigma^{(1)}_{\beta\alpha}(\mathbf{k},\omega) = B_{\mathbf{k}}. \tag{A5b}$$

The second-order self-energy terms originate from the Feynman diagrams in Figs. 10(b), (c), and (d). The coefficients $\mathcal{C}_{1\mathbf{k}}$ and $\mathcal{C}_{2\mathbf{k}}$ stem from the normal-ordering of $\mathcal{H}_2$. The complete expressions read

$$\begin{aligned}
\Sigma^{(2)}_{\alpha\alpha}(\mathbf{k},\omega) \;&=\; \Sigma^{(2)}_{\beta\beta}(\mathbf{k},\omega) = \mathcal{C}_{1\mathbf{k}} + \Big(\frac{2}{N}\Big)\sum_{\mathbf{p}} (\ell_{\mathbf{k}}\ell_{\mathbf{p}})^2 \frac{B_{\mathbf{p}}(V^{(2)}_{\mathbf{k},\mathbf{p},\mathbf{p},\mathbf{k}} + V^{(3)}_{\mathbf{k},\mathbf{p},\mathbf{p},\mathbf{k}})}{2E_{\mathbf{p}}} \\
&+\; \Big(\frac{2}{N}\Big)^2 \sum_{\mathbf{pq}} 2(\ell_{\mathbf{p}}\ell_{\mathbf{q}}\ell_{\mathbf{k}}\ell_{[\mathbf{k}+\mathbf{p}-\mathbf{q}]})^2 \Big[\frac{V^{(2)}_{\mathbf{k},\mathbf{p},\mathbf{q},[\mathbf{k}+\mathbf{p}-\mathbf{q}]} V^{(3)}_{[\mathbf{k}+\mathbf{p}-\mathbf{q}],\mathbf{q},\mathbf{p},\mathbf{k}}}{\omega - E_{\mathbf{p}} - E_{\mathbf{q}} - E_{[\mathbf{k}+\mathbf{p}-\mathbf{q}]} + i\delta} \\
&-\; \frac{V^{(7)}_{\mathbf{k},\mathbf{p},\mathbf{q},[\mathbf{k}+\mathbf{p}-\mathbf{q}]} V^{(8)}_{[\mathbf{k}+\mathbf{p}-\mathbf{q}],\mathbf{q},\mathbf{p},\mathbf{k}}}{\omega + E_{\mathbf{p}} + E_{\mathbf{q}} + E_{[\mathbf{k}+\mathbf{p}-\mathbf{q}]} - i\delta}\Big], \qquad \text{(A6a)} \\
\Sigma^{(2)}_{\alpha\beta}(\mathbf{k},\omega) \;&=\; \Sigma^{(2)}_{\beta\alpha}(\mathbf{k},\omega) = \mathcal{C}_{2\mathbf{k}} + \Big(\frac{2}{N}\Big)^2 \sum_{\mathbf{pq}} 2(\ell_{\mathbf{p}}\ell_{\mathbf{q}}\ell_{\mathbf{k}}\ell_{[\mathbf{k}+\mathbf{p}-\mathbf{q}]})^2 \times \\
&\Big[\frac{V^{(2)}_{\mathbf{k},\mathbf{p},\mathbf{q},[\mathbf{k}+\mathbf{p}-\mathbf{q}]} V^{(7)}_{[\mathbf{k}+\mathbf{p}-\mathbf{q}],\mathbf{q},\mathbf{p},\mathbf{k}}}{\omega - E_{\mathbf{p}} - E_{\mathbf{q}} - E_{[\mathbf{k}+\mathbf{p}-\mathbf{q}]} + i\delta} - \frac{V^{(7)}_{\mathbf{k},\mathbf{p},\mathbf{q},[\mathbf{k}+\mathbf{p}-\mathbf{q}]} V^{(5)}_{[\mathbf{k}+\mathbf{p}-\mathbf{q}],\mathbf{q},\mathbf{p},\mathbf{k}}}{\omega + E_{\mathbf{p}} + E_{\mathbf{q}} + E_{[\mathbf{k}+\mathbf{p}-\mathbf{q}]} - i\delta}\Big], \qquad \text{(A6b)}
\end{aligned}$$

where $[\mathbf{k}+\mathbf{p}-\mathbf{q}]$ is meant to be mapped to $(\mathbf{k}+\mathbf{p}-\mathbf{q})$ in the first BZ by an appropriate reciprocal vector $\mathbf{G}$. In deriving Eqs. (A6a) and (A6b) we have used the symmetry properties of the vertices, see Eq. (B2).

Appendix B: Vertex factors

The expressions for the vertex factors are very lengthy. It is convenient to first define the following functions

$$
\begin{aligned}
\mathcal{J}_1 &= \gamma_2(1-4)+\gamma_2(2-4)+\gamma_2(1-3)+\gamma_2(2-3)-\gamma_2(1)-\gamma_2(2)-\gamma_2(1-3-4) \\
&- \gamma_2(2-3-4), \\
\mathcal{J}_2 &= \gamma_2(1-4)+\gamma_2(2-4)+\gamma_2(1-3)+\gamma_2(2-3), \\
\mathcal{S}_1 &= \gamma_x(4)\gamma_y(2-4)+\gamma_x(1+2-4)\gamma_y(1-4)+\gamma_x(1-3)\gamma_y(1+2-3)+\gamma_x(2-3)\gamma_y(3) \\
&+ \gamma_x(3)\gamma_y(2-3)+\gamma_x(1+2-3)\gamma_y(1-3)+\gamma_x(1-4)\gamma_y(1+2-4)+\gamma_x(2-4)\gamma_y(4), \\
\mathcal{S}_2 &= \gamma_x(4)\gamma_y(1-4)+\gamma_x(1+2-4)\gamma_y(2-4)+\gamma_x(2-3)\gamma_y(1+2-3)+\gamma_x(1-3)\gamma_y(3) \\
&+ \gamma_x(3)\gamma_y(1-3)+\gamma_x(1+2-3)\gamma_y(2-3)+\gamma_x(2-4)\gamma_y(1+2-4)+\gamma_x(1-4)\gamma_y(4), \\
\mathcal{S}_3 &= \gamma_x(1-3-4)\gamma_y(2-4)+\gamma_x(1)\gamma_y(2-3)+\gamma_x(1-4)\gamma_y(2-3-4)+\gamma_x(1-3)\gamma_y(2) \\
&+ \gamma_x(2-3-4)\gamma_y(1-4)+\gamma_x(2)\gamma_y(1-3)+\gamma_x(2-4)\gamma_y(1-3-4)+\gamma_x(2-3)\gamma_y(1), \\
\mathcal{S}_4 &= \gamma_x(1-3-4)\gamma_y(2-3)+\gamma_x(1)\gamma_y(2-4)+\gamma_x(1-3)\gamma_y(2-3-4)+\gamma_x(1-4)\gamma_y(2) \\
&+ \gamma_x(2-3-4)\gamma_y(1-3)+\gamma_x(2)\gamma_y(1-4)+\gamma_x(2-3)\gamma_y(1-3-4)+\gamma_x(2-4)\gamma_y(1), \\
\mathcal{S}_5 &= \gamma_x(2)\gamma_y(2-3)+\gamma_x(2-3-4)\gamma_y(2-4)+\gamma_x(1-4)\gamma_y(1-3-4)+\gamma_x(1-3)\gamma_y(1) \\
&+ \gamma_x(1)\gamma_y(1-3)+\gamma_x(1-3-4)\gamma_y(1-4)+\gamma_x(2-4)\gamma_y(2-3-4)+\gamma_x(2-3)\gamma_y(2), \\
\mathcal{S}_6 &= \gamma_x(2)\gamma_y(2-4)+\gamma_x(2-3-4)\gamma_y(2-3)+\gamma_x(1-3)\gamma_y(1-3-4)+\gamma_x(1-4)\gamma_y(1) \\
&+ \gamma_x(1)\gamma_y(1-4)+\gamma_x(1-3-4)\gamma_y(1-3)+\gamma_x(2-3)\gamma_y(2-3-4)+\gamma_x(2-4)\gamma_y(2), \\
\mathcal{S}_7 &= \gamma_x(1+2-3)\gamma_y(1-4)+\gamma_x(3)\gamma_y(2-4)+\gamma_x(1-3)\gamma_y(1+2-4)+\gamma_x(2-3)\gamma_y(4) \\
&+ \gamma_x(1+2-4)\gamma_y(1-3)+\gamma_x(4)\gamma_y(2-3)+\gamma_x(1-4)\gamma_y(1+2-3)+\gamma_x(2-4)\gamma_y(3), \\
\mathcal{S}_8 &= \gamma_x(1+2-3)\gamma_y(2-4)+\gamma_x(3)\gamma_y(1-4)+\gamma_x(2-3)\gamma_y(1+2-4)+\gamma_x(1-3)\gamma_y(4) \\
&+ \gamma_x(1+2-4)\gamma_y(2-3)+\gamma_x(4)\gamma_y(1-3)+\gamma_x(2-4)\gamma_y(1+2-3)+\gamma_x(1-4)\gamma_y(3), \\
\mathcal{S}_9 &= \gamma_x(1-4)\gamma_y(2-4)+\gamma_x(1-3)\gamma_y(2-3)+\gamma_x(2-4)\gamma_y(1-4)+\gamma_x(2-3)\gamma_y(1-3), \\
\mathcal{S}_{10} &= \gamma_x(2-3)\gamma_y(2-4)+\gamma_x(1-3)\gamma_y(1-4)+\gamma_x(2-4)\gamma_y(2-3)+\gamma_x(1-4)\gamma_y(1-3), \\
\mathcal{S}_{11} &= \gamma_x(2)\gamma_y(4)+\gamma_x(4)\gamma_y(2)+\gamma_x(1+2-3)\gamma_y(1-3-4)+\gamma_x(1-3-4)\gamma_y(1+2-3) \\
&+ \gamma_x(1+2-4)\gamma_y(1)+\gamma_x(1)\gamma_y(1+2-4)+\gamma_x(2-3-4)\gamma_y(3)+\gamma_x(3)\gamma_y(2-3-4), \\
\mathcal{S}_{12} &= \gamma_x(2)\gamma_y(3)+\gamma_x(3)\gamma_y(2)+\gamma_x(1+2-4)\gamma_y(1-3-4)+\gamma_x(1-3-4)\gamma_y(1+2-4) \\
&+ \gamma_x(1+2-3)\gamma_y(1)+\gamma_x(1)\gamma_y(1+2-3)+\gamma_x(2-3-4)\gamma_y(4)+\gamma_x(4)\gamma_y(2-3-4),
\end{aligned}
$$

$$
\begin{aligned}
\mathcal{S}_{13} &= \gamma_x(1)\gamma_y(4) + \gamma_x(4)\gamma_y(1) + \gamma_x(1+2-3)\gamma_y(2-3-4) + \gamma_x(2-3-4)\gamma_y(1+2-3) \\
&+ \gamma_x(1+2-4)\gamma_y(2) + \gamma_x(2)\gamma_y(1+2-4) + \gamma_x(1-3-4)\gamma_y(3) + \gamma_x(3)\gamma_y(1-3-4), \\
\mathcal{S}_{14} &= \gamma_x(1)\gamma_y(3) + \gamma_x(3)\gamma_y(1) + \gamma_x(1+2-4)\gamma_y(2-3-4) + \gamma_x(2-3-4)\gamma_y(1+2-4) \\
&+ \gamma_x(1+2-3)\gamma_y(2) + \gamma_x(2)\gamma_y(1+2-3) + \gamma_x(1-3-4)\gamma_y(4) + \gamma_x(4)\gamma_y(1-3-4).
\end{aligned}
$$

The vertex factors required for our calculations are

$$
\begin{aligned}
V^{(2)}_{12;34} &= \Big[- x_3\gamma_1(2-3) - x_4\gamma_1(2-4) - x_1x_2x_3\gamma_1(1-3) - x_1x_2x_4\gamma_1(1-4) \\
&+ x_1x_2\gamma_1(1) + \gamma_1(2) + x_1x_2x_3x_4\gamma_1(1-3-4) + x_3x_4\gamma_1(2-3-4)\Big] \\
&+ \Big(\frac{\eta-2\mu}{1+\zeta-8\mu}\Big)\Big[x_2 + \Phi_G x_1x_3x_4\Big]\mathcal{J}_1 \\
&- \Big(\frac{4\mu}{1+\zeta-8\mu}\Big)\Big[- (x_2 + \Phi_G x_3x_4)\mathcal{J}_2 + \frac{1}{2}(\mathcal{S}_1 + x_1x_2\mathcal{S}_2 + x_1x_3\mathcal{S}_3 + x_1x_4\mathcal{S}_4 \\
&+ x_2x_3\mathcal{S}_5 + x_2x_4\mathcal{S}_6 + x_3x_4\mathcal{S}_7 + x_1x_2x_3x_4\mathcal{S}_8 - 2x_1\mathcal{S}_9 - 2x_2x_3x_4\mathcal{S}_{10} - x_4\mathcal{S}_{11} \\
&- x_3\mathcal{S}_{12} - x_1x_2x_4\mathcal{S}_{13} - x_1x_2x_3\mathcal{S}_{14})\Big]. \qquad \text{(B1a)} \\
V^{(3)}_{12;34} &= \Big[- x_1\gamma_1(1-3) - x_2\gamma_1(2-3) - x_1x_3x_4\gamma_1(1-4) - x_2x_3x_4\gamma_1(2-4) \\
&+ x_1x_3\gamma_1(1) + x_2x_3\gamma_1(2) + x_1x_4\gamma_1(1-3-4) + x_2x_4\gamma_1(2-3-4)\Big] \\
&+ \Big(\frac{\eta-2\mu}{1+\zeta-8\mu}\Big)\Big[x_3 + \Phi_G x_1x_2x_4\Big]\mathcal{J}_1 \\
&- \Big(\frac{4\mu}{1+\zeta-8\mu}\Big)\Big[- (x_3 + \Phi_G x_1x_2x_4)\mathcal{J}_2 + \frac{1}{2}(x_2x_3\mathcal{S}_1 + x_1x_3\mathcal{S}_2 + x_1x_2\mathcal{S}_3 + x_1x_2x_3x_4\mathcal{S}_4 \\
&+ \mathcal{S}_5 + x_3x_4\mathcal{S}_6 + x_2x_4\mathcal{S}_7 + x_1x_4\mathcal{S}_8 - 2x_1x_2x_3\mathcal{S}_9 - 2x_4\mathcal{S}_{10} - x_2x_3x_4\mathcal{S}_{11} \\
&- x_2\mathcal{S}_{12} - x_1x_3x_4\mathcal{S}_{13} - x_1\mathcal{S}_{14})\Big]. \qquad \text{(B1b)} \\
V^{(5)}_{12;34} &= \Big[- x_2x_3x_4\gamma_1(1-3) - x_1x_3x_4\gamma_1(2-3) - x_1\gamma_1(2-4) - x_2\gamma_1(1-4) \\
&+ x_1x_4\gamma_1(2) + x_2x_4\gamma_1(1) + x_1x_3\gamma_1(2-3-4) + x_2x_3\gamma_1(1-3-4)\Big] \\
&+ \Big(\frac{\eta-2\mu}{1+\zeta-8\mu}\Big)\Big[x_1x_2x_4 + \Phi_G x_3\Big]\mathcal{J}_1 \\
&- \Big(\frac{4\mu}{1+\zeta-8\mu}\Big)\Big[- (x_1x_2x_4 + \Phi_G x_3)\mathcal{J}_2 + \frac{1}{2}(x_1x_4\mathcal{S}_1 + x_2x_4\mathcal{S}_2 + x_3x_4\mathcal{S}_3 + \mathcal{S}_4 \\
&+ x_1x_2x_3x_4\mathcal{S}_5 + x_1x_2\mathcal{S}_6 + x_1x_3\mathcal{S}_7 + x_2x_3\mathcal{S}_8 - 2x_4\mathcal{S}_9 - 2x_1x_2x_3\mathcal{S}_{10} - x_1\mathcal{S}_{11} \\
&- x_1x_3x_4\mathcal{S}_{12} - x_2\mathcal{S}_{13} - x_2x_3x_4\mathcal{S}_{14})\Big]. \qquad \text{(B1c)}
\end{aligned}
$$

$$
\begin{aligned}
V^{(7)}_{12;34} &= \Big[x_1x_4\gamma_1(1-3)+x_1x_3\gamma_1(1-4)+x_2x_3\gamma_1(2-4)+x_2x_4\gamma_1(2-3)\\
&- x_1x_3x_4\gamma_1(1)-x_2x_3x_4\gamma_1(2)-x_1\gamma_1(1-3-4)-x_2\gamma_1(2-3-4)\Big]\\
&+ \Big(\frac{\eta-2\mu}{1+\zeta-8\mu}\Big)\Big[-x_3x_4-\Phi_G x_1x_2\Big]\mathcal{J}_1\\
&- \Big(\frac{4\mu}{1+\zeta-8\mu}\Big)\Big[(x_3x_4+\Phi_G x_1x_2)\mathcal{J}_2+\frac{1}{2}(-x_2x_3x_4\mathcal{S}_1-x_1x_3x_4\mathcal{S}_2-x_1x_2x_4\mathcal{S}_3\\
&- x_1x_2x_3\mathcal{S}_4-x_4\mathcal{S}_5-x_3\mathcal{S}_6-x_2\mathcal{S}_7-x_1\mathcal{S}_8+2x_1x_2x_3x_4\mathcal{S}_9+2\mathcal{S}_{10}+x_2x_3\mathcal{S}_{11}\\
&+ x_2x_4\mathcal{S}_{12}+x_1x_3\mathcal{S}_{13}+x_1x_4\mathcal{S}_{14})\Big]. \qquad \text{(B1d)}\\
V^{(8)}_{12;34} &= \Big[x_1x_4\gamma_1(2-4)+x_2x_4\gamma_1(1-4)+x_1x_3\gamma_1(2-3)+x_2x_3\gamma_1(1-3)\\
&- x_1\gamma_1(2)-x_2\gamma_1(1)-x_1x_3x_4\gamma_1(2-3-4)-x_2x_3x_4\gamma_1(1-3-4)\Big]\\
&+ \Big(\frac{\eta-2\mu}{1+\zeta-8\mu}\Big)\Big[-x_1x_2-\Phi_G x_3x_4\Big]\mathcal{J}_1\\
&- \Big(\frac{4\mu}{1+\zeta-8\mu}\Big)\Big[(x_1x_2+\Phi_G x_3x_4)\mathcal{J}_2+\frac{1}{2}(-x_1\mathcal{S}_1-x_2\mathcal{S}_2-x_3\mathcal{S}_3-x_4\mathcal{S}_4\\
&- x_1x_2x_3\mathcal{S}_5-x_1x_2x_4\mathcal{S}_6-x_1x_3x_4\mathcal{S}_7-x_2x_3x_4\mathcal{S}_8+2\mathcal{S}_9+2x_1x_2x_3x_4\mathcal{S}_{10}\\
&+ x_1x_4\mathcal{S}_{11}+x_1x_3\mathcal{S}_{12}+x_2x_4\mathcal{S}_{13}+x_2x_3\mathcal{S}_{14})\Big], \qquad \text{(B1e)}
\end{aligned}
$$

where $\Phi_G = \exp(iG_x)$, G_x being the x-component of the reciprocal lattice vector $\mathbf{G}$ appearing in the momentum conserving delta-function in Eq. (9). These vertex factors fulfill the following symmetry relations

$$
\begin{aligned}
V^{(2)}_{12;34} &= V^{(2)}_{12;43}; \quad V^{(3)}_{12;34} = V^{(3)}_{21;34}; \quad V^{(5)}_{12;34} = V^{(5)}_{21;34}, \qquad \text{(B2a)}\\
V^{(7)}_{12;34} &= V^{(7)}_{21;34} = V^{(7)}_{12;43}; \quad V^{(8)}_{12;34} = V^{(8)}_{21;34} = V^{(8)}_{12;43}. \qquad \text{(B2b)}
\end{aligned}
$$

If no reciprocal lattice vector is involved in the momentum conservation, i.e., $\mathbf{G} = 0$, there are some additional symmetries

$$
V^{(3)}_{12;34} = V^{(5)}_{12;34}; \quad V^{(7)}_{12;34} = V^{(8)}_{12;34}. \qquad \text{(B2c)}
$$

Appendix C: Coefficients $\mathcal{C}_{1\mathbf{k}}$ and $\mathcal{C}_{2\mathbf{k}}$

We define the functions $\mathcal{P}_{\mathbf{k}}$ and $\mathcal{Q}_{\mathbf{k}}$

$$
\begin{aligned}
\mathcal{P}_{\mathbf{k}} \;=\; & \Big(\frac{2}{N}\Big)^2 \sum_{12} 2\ell_1^2\ell_2^2\Big[x_1^2x_2^2\Big\{6+6\gamma_2(k)+6\gamma_2(2)+2\gamma_2(k-2)+\gamma_x(1-2)\gamma_y(1+2)\\
&+\;\gamma_x(k-1-2)\gamma_y(k-1+2)\Big\}+x_1^2\Big\{2\gamma_2(k-2)+6\gamma_2(2)+\gamma_x(k+1-2)\gamma_y(k-1-2)\\
&+\;\gamma_x(k-1-2)\gamma_y(k+1-2)+\gamma_x(k-1+2)\gamma_y(k-1-2)+\gamma_x(k-1+2)\gamma_y(k+1-2)\Big\}\\
&+\;x_1x_2\Big\{4\gamma_x(k-1)\gamma_y(k-2)+4\gamma_x(k-2)\gamma_y(k-1)+4\gamma_x(1)\gamma_y(2)+4\gamma_x(2)\gamma_y(1)\\
&+\;6\gamma_x(1-2)+6\gamma_y(1-2)+4\gamma_x(k)\gamma_y(k-1-2)+4\gamma_x(k-1-2)\gamma_y(k)\Big\}\\
&-\;x_1^2x_2\Big\{8\gamma_x(k)\gamma_y(k-2)+8\gamma_x(k-2)\gamma_y(k)+12\gamma_x(2)+12\gamma_y(2)+4\gamma_x(1)\gamma_y(1-2)+\\
&+\;4\gamma_x(1-2)\gamma_y(1)+2\gamma_x(k-1)\gamma_y(k-1-2)+2\gamma_x(k-1-2)\gamma_y(k-1)\\
&+\;2\gamma_x(k+1-2)\gamma_y(k-1)+2\gamma_x(k-1)\gamma_y(k+1-2)\Big\}\\
&-\;x_1\Big\{4\gamma_x(2)\gamma_y(1-2)+4\gamma_x(1-2)\gamma_y(2)+2\gamma_x(k-2)\gamma_y(k-1+2)\\
&+\;2\gamma_x(k-1+2)\gamma_y(k-2)+2\gamma_x(k+1-2)\gamma_y(k-2)+2\gamma_x(k-2)\gamma_y(k+1-2)\Big\}\\
&+\;\Big\{\gamma_x(1-2)\gamma_y(1+2)+\gamma_x(k-1-2)\gamma_y(k+1-2)\Big\}\Big]. \qquad \text{(C1a)}\\
\mathcal{Q}_{\mathbf{k}} \;=\; & \Big(\frac{2}{N}\Big)^2 \sum_{12} 2\ell_1^2\ell_2^2\Big[x_1^2x_2^2\Big\{6\gamma_x(k)+6\gamma_y(k)+4\gamma_x(2)\gamma_y(k-2)+4\gamma_x(k-2)\gamma_y(2)\\
&+\;\gamma_x(k-1-2)\gamma_y(1-2)+\gamma_x(1-2)\gamma_y(k-1-2)\Big\}\\
&+\;x_1^2\Big\{4\gamma_x(2)\gamma_y(k-2)+4\gamma_x(k-2)\gamma_y(2)+\gamma_x(k+1-2)\gamma_y(1-2)\\
&+\;\gamma_x(1-2)\gamma_y(k+1-2)+\gamma_x(k-1+2)\gamma_y(1-2)+\gamma_x(1-2)\gamma_y(k-1+2)\Big\}\\
&+\;x_1x_2\Big\{8\gamma_x(2)\gamma_y(k-1)+8\gamma_x(k-1)\gamma_y(2)+6\gamma_x(k-1+2)+6\gamma_y(k-1+2)\\
&+\;4\gamma_x(k)\gamma_y(1-2)+4\gamma_x(1-2)\gamma_y(k)\Big\}\\
&-\;x_1^2x_2\Big\{8\gamma_x(k)\gamma_y(2)+8\gamma_x(2)\gamma_y(k)+12\gamma_x(k-2)+12\gamma_y(k-2)+4\gamma_x(k-1)\gamma_y(1-2)+\\
&+\;4\gamma_x(1-2)\gamma_y(k-1)+4\gamma_x(k-1-2)\gamma_y(1)+4\gamma_x(1)\gamma_y(k-1-2)\Big\}\\
&-\;x_1\Big\{4\gamma_x(k-2)\gamma_y(1-2)+4\gamma_x(1-2)\gamma_y(k-2)+4\gamma_x(2)\gamma_y(k-1-2)\\
&+\;4\gamma_x(k-1-2)\gamma_y(2)\Big\}+\Big\{\gamma_x(1-2)\gamma_y(k-1-2)+\gamma_x(k-1-2)\gamma_y(1-2)\Big\}\Big]. \qquad \text{(C1b)}
\end{aligned}
$$

Then, the static second-order corrections are given by

$$\mathcal{C}_{1\mathbf{k}} = (\ell_{\mathbf{k}}^2 + m_{\mathbf{k}}^2)\mathcal{Q}_{\mathbf{k}} + 2\ell_{\mathbf{k}} m_{\mathbf{k}} \mathcal{P}_{\mathbf{k}}, \tag{C2a}$$

$$\mathcal{C}_{2\mathbf{k}} = (\ell_{\mathbf{k}}^2 + m_{\mathbf{k}}^2)\mathcal{P}_{\mathbf{k}} + 2\ell_{\mathbf{k}} m_{\mathbf{k}} \mathcal{Q}_{\mathbf{k}}. \tag{C2b}$$

---

* Electronic address: majumdak@gvsu.edu

† Electronic address: furtond@gvsu.edu

‡ Electronic address: goetz.uhrig@tu-dortmund.de

[1] R. Coldea, S. M. Hayden, G. Aeppli, T. G. Perring, C. D. Frost, T. E. Mason, S. W. Cheong, and Z. Fisk, Phys. Rev. Lett. **86**, 5377 (2001).

[2] N. S. Headings, S. M. Hayden, R. Coldea, and T. G. Perring, Phys. Rev. Lett. **105**, 247001 (2010).

[3] H. M. Ronnow, D. F. McMorrow, R. Coldea, A. Harrison, I. D. Youngson, T. G. Perring, G. Aeppli, O. Syljuasen, K. Lefmann, and C. Rischel, Phys. Rev. Lett. **87**, 037202 (2001).

[4] N. B. Christensen, D. F. McMorrow, H. M. Ronnow, A. Harrison, T. G. Perring, and R. Coldea, J. Magn. Magn. Mater. **272-276**, 896 (2004).

[5] N. B. Christensen, H. M. Ronnow, D. F. McMorrow, A. Harrison, T. G. Perring, M. Enderle, R. Coldea, L. P. Regnault, and G. Aeppli, Proc. Natl. Acad. Sci. U.S.A. **104**, 15264 (2007).

[6] A. Bombardi, J. Rodriguez-Carvajal, S. D. Matteo, F. de Bergevin, L. Paolasini, P. Carretta, P. Millet, and R. Caciuffo, Phys. Rev. Lett. **93**, 027202 (2004).

[7] R. Melzi, P. Carretta, A. Lascialfari, M. Mambrini, M. Troyer, P. Millet, and F. Mila, Phys. Rev. Lett. **85**, 1318 (2000).

[8] R. Melzi, S. Aldrovandi, F. Tedoldi, P. Carretta, P. Millet, and F. Mila, Phys. Rev. B **64**, 024409 (2001).

[9] P. Carretta, N. Papinutto, C. B. Azzoni, M. C. Mozzati, E. Pavarini, S. Gonthier, and P. Millet, Phys. Rev. B **66**, 094420 (2002).

[10] M. L. Tacon, G. Ghiringhelli, J. Chaloupka, M. M. Sala, V. Hinkov, M. Haverkort, M. Minola, M. Bakr, K. J. Zhou, S. Blanco-Canosa, et al., Nature Phys. **7**, 725 (2011).

[11] H. T. Diep, *Frustrated Spin Systems* (World Scientific, Singapore, 2004), 1st ed.

[12] S. Brehmer, H. J. Mikeska, and M. Muller, Phys. Rev. B **60**, 329 (1999).

[13] E. Pavarini, S. C. Tarantino, T. B. Ballaran, M. Zema, P. Ghigna, and P. Carretta, Phys. Rev. B **77**, 014425 (2008).

[14] M. Roger and J. M. Delrieu, Phys. Rev. B **39**, 2299 (1989).

[15] H. J. Schmidt and Y. Kuramoto, Physica C **167**, 263 (1990).

[16] A. Chubukov, E. Gagliano, and C. Balseiro, Phys. Rev. B **45**, 7889 (1992).

[17] J. G. Bednorz and K. A. Müller, Z. Phys. B **64**, 189 (1986).

[18] Y. Mizuno, T. Tohyama, and S. Maekawa, J. Low Temp. Phys. **117**, 389 (1999).

[19] E. Müller-Hartmann and A. Reischl, Eur. Phys. J. B **28**, 173 (2002).

[20] C. J. Calzado, C. de Graaf, E. Bordas, R. Caballol, and J.-P. Malrieu, Phys. Rev. B **67**, 132409 (2003).

[21] M. Takahashi, J. Phys. C **10**, 1289 (1977).

[22] A. H. MacDonald, S. M. Girvin, and D. Yoshioka, Phys. Rev. B **37**, 9753 (1988).

[23] A. Reischl, E. Müller-Hartmann, and G. S. Uhrig, Phys. Rev. B **70**, 245124 (2004).

[24] S. A. Hamerla, S. Duffe, and G. S. Uhrig, Phys. Rev. B **82**, 235117 (2010).

[25] J. Lorenzana, J. Eroles, and S. Sorella, Phys. Rev. Lett. **83**, 5122 (1999).

[26] A. A. Katanin and A. P. Kampf, Phys. Rev. B **67**, 100404 (2003).

[27] K. P. Schmidt, A. Gössling, U. Kuhlmann, C. Thomsen, A. Löffert, C. Gross, and W. Assmus, Phys. Rev. B **72**, 094419 (2005).

[28] A. A. Katanin and A. P. Kampf, Phys. Rev. B **66**, 100403 (R) (2002).

[29] G. S. Uhrig, K. P. Schmidt, and M. Grüninger, Phys. Rev. Lett. **93**, 267003 (2004).

[30] M. Matsuda, K. Katsymata, R. S. Eccleston, S. Brehmer, and H. J. Mikeska, Phys. Rev. B **62**, 8903 (2002).

[31] T. Nunner, P. Brune, T. Kopp, M. Windt, and M. Gruninger, Phys. Rev. B **66**, 180404 (2002).

[32] K. P. Schmidt and G. S. Uhrig, Mod. Phys. Lett. B **19**, 1179 (2005).

[33] S. Notbohm, P. Ribeiro, B. Lake, D. A. Tennant, K. P. Schmidt, G. S. Uhrig, C. Hess, R. Klingeler, G. Behr, B. Büchner, et al., Phys. Rev. Lett. **98**, 027403 (2007).

[34] Y. Kamihara, T. Watanabe, M. Hirano, and H. Hosono, J. Am. Chem. Soc. **130**, 3296 (2008).

[35] C. de la Cruz, Q. Huang, J. W. Lynn, J. Li, W. R. II, J. L. Zarestky, H. A. Mook, G. F. Chen, J. L. Luo, N. L. Wang, et al., Nature **453**, 899 (2008).

[36] H.-H. Klaus, H. Luetkens, R. Klingeler, C. Hess, F. J. Litterst, M. Kraken, M. M. Korshunov, I. Eremin, S.-L. Drechsler, R. Khasanov, et al., Phys. Rev. Lett. **101**, 077005 (2008).

[37] J. Dong, H. J. Zhang, G. Xu, Z. Li, G. Li, W. Z. H. abd D. Wu, G. F. Chen, X. Dai, J. L. Luo, Z. Fang, et al., Europhys. Lett. **83**, 27006 (2008).

[38] J. Zhao, D. X. Yao, S. Li, T. Hong, Y. Chen, S. Chang, W. R. II, J. W. Lynn, H. A. Mook, G. F. Chen, et al., Phys. Rev. Lett. **101**, 167203 (2008).

[39] S. O. Diallo, V. P. Antropov, T. G. Perring, C. Broholm, J. J. Pulikkotil, N. Ni, S. L. Budko, P. C. Canfield, A. Kreyssig, A. I. Goldman, et al., Phys. Rev. Lett. **102**, 187206 (2009).

[40] J. Zhao, D. T. Adroja, D.-X. Yao, R. Bewley, S. Li, X. F. Wang, G. Wu, X. H. Chen, J. Hu, and P. Dai, Nature Phys. **5**, 555 (2009).

[41] Q. Si and E. Abrahams, Phys. Rev. Lett. **101**, 076401 (2008).

[42] D. X. Yao and E. W. Carlson, Phys. Rev. B **78**, 052507 (2008).

[43] G. S. Uhrig, M. Holt, J. Oitmaa, O. P. Sushkov, and R. R. P. Singh, Phys. Rev. B **79**, 092416 (2009).

[44] R. R. P. Singh, Supercond. Sci. Technol. **22**, 015005 (2009).

[45] R. Applegate, J. Oitmaa, and R. R. P. Singh, Phys. Rev. B **81**, 024505 (2010).

[46] D. X. Yao and E. W. Carlson, Front. Phys. China **5**, 166 (2010).

[47] M. Holt, O. P. Sushkov, D. Stanek, and G. S. Uhrig, Phys. Rev. B **83**, 144528 (2011).

[48] K. Majumdar, J. Phys. Cond. Mat. **23**, 116004 (2011).

[49] M. J. Han, Q. Yin, W. E. Pickett, and S. Y. Savrasov, Phys. Rev. Lett. **102**, 107003 (1992).

[50] F. Krüger, S. Kumar, J. Zaanen, and J. van den Brink, Phys. Rev. B **79**, 054504 (2009).

[51] R. R. P. Singh, arXiv:0903.4408 (2009).

[52] A. N. Yaresko, G.-Q. Liu, V. N. Antonov, and O. K. Andersen, Phys. Rev. B **79**, 144421 (2009).

[53] A. L. Wysocki, K. D. Belashchenko, and V. P. Antropov, Nat. Phys. **7**, 485 (2011).

[54] D. Stanek, O. P. Sushkov, and G. S. Uhrig, Phys. Rev. B **84**, 064505 (2011).

[55] R. Yu, Z. Wang, P. Goswami, A. Nevidomskyy, Q. Si, and E. Abrahams, arXiv:1112.4785 (2012).

[56] A. A. Tsirlin and H. Rosner, Phys. Rev. B **79**, 214417 (2009).

[57] O. Volkova, I. Morozov, V. Shutov, E. Lapsheva, P. Sindzingre, O. Cépas, M. Yehia, V. Kataev, R. Klingeler, B. Búchner, et al., Phys. Rev. B **82**, 054413 (2010).

[58] J. I. Igarashi, Phys. Rev. B **46**, 10763 (1992).

[59] J. I. Igarashi and T. Nagao, Phys. Rev. B **72**, 014403 (2005).

[60] K. Majumdar, Phys. Rev. B **82**, 144407 (2010).

[61] J. Oitmaa and Z. Weihong, Phys. Rev. B **54**, 3022 (1996).

[62] R. F. Bishop, P. H. Y. Li, R. Darradi, and J. Richter, Europhys. Lett. **83**, 47004 (2008).

[63] R. R. P. Singh, Z. Weihong, C. J. Hamer, and J. Oitmaa, Phys. Rev. B **60**, 7278 (1999).

[64] O. P. Sushkov, J. Oitmaa, and W. Zheng, Phys. Rev. B **63**, 104420 (2001).

[65] J. Sirker, Z. Weihong, O. P. Sushkov, and J. Oitmaa, Phys. Rev. B **73**, 184420 (2006).

[66] A. A. Nersesyan and A. M. Tsvelik, Phys. Rev. B **67**, 024422 (2003).

[67] C. J. Hamer, W. Zheng, and P. Arndt, Phys. Rev. B **46**, 6276 (1992).

[68] W. Zheng and C. J. Hamer, Phys. Rev. B **47**, 7961 (1993).

[69] A. V. Syromyatnikov, J. Phys: Condens. Matter **22**, 216003 (2010).

[70] R. R. P. Singh and M. P. Gelfand, Phys. Rev. B **52**, 15695 (1995).

[71] W. Zheng, J. Oitmaa, and C. J. Hamer, Phys. Rev. B **71**, 184440 (2005).

[72] A. W. Sandvik and R. R. P. Singh, Phys. Rev. Lett. **86**, 528 (2001).